Middle to Late Triassic (late Ladinian – late Carnian) palynology of the shallow stratigraphic core 7534/4-U-1, Sentralbanken High, Northern Barents Sea

Johne Landa

Thesis for master degree in Petroleum Geoscience

Department of Earth Science,
University of Bergen

September, 2015

Abstract

In the Triassic period, a large seaway developed on the northern coast of Pangea, in the area which is the present-day Barents Sea. Deposition of sediment sourced from the Uralian Mountains in-filled this sea during the Late Triassic, forming a large prograding delta which gradually converted into a paralic platform. Very little palynological data are available from the northern Barents Sea due to the remoteness of the region. Several stratigraphic cores drilled by the Norwegian Petroleum Directorate in the area therefore provide important insights into the palaeogeography and depositional history of sediments in this part of the Barents Shelf. This study forms a part of a broader palynological investigation of the Middle to Late Triassic succession of the Barents Sea currently being undertaken at the University of Bergen. In the present study, palynological samples were collected from a shallow stratigraphic core, 7534/4-U-1, drilled in the Sentralbanken High in the Northern Barents Sea. The core penetrates approximately 230m of the De Geerdalen Formation (Snadd Formation equivalent), and the hypothesis, based on seismic, was that the Ladinian – Carnian transition should be recorded within this core. 56 samples were analyzed for palynostratigraphy and palynofacies. Investigation of this core reveals three distinct assemblages, assigned to range from late Ladinian to mid-late Carnian age. A palynomorph assemblage dominated by the monolete fern spore taxon *Leschikisporis aduncus* is the most prominent feature within this succession; similar assemblages have previously been documented from late Carnian deposits in the region. The palynofloral distribution and dominance of terrestrial kerogen is consistent with deposition close to fern dominated delta/coastal plain swamp. However, the sporadic presence of acritarchs and prasinophytes is indicative of episodic marine influence.

Acknowledgements

I would like to express my very great appreciation to my supervisor Gunn Mangerud and co-supervisor Niall William Paterson at UiB. Thank you for the valuable discussions and support over the last two years. My special thanks are extended to Gunn Mangerud for funding the conference-trip to Svalbard.

I also wish to acknowledge the help provided by Bjørn Anders Lundschien at the NPD during the core logging.

This study has been funded by a FORCE industry consortium by the following companies: A/S Norske Shell, Centrica Energy, Chevron Norge AS, ConocoPhillips Skandinavia AS, Det Norske Oljeselskap ASA, Dong E&P Norge AS, ENI Norge AS, Lundin Norway AS and Statoil Petroleum AS. Thank you for financing this project.

Table of Contents

1. Introduction

Palynostratigraphic research of the Middle to Late Triassic has in recent time been used extensively in the Barents Sea region. Accordingly, such strata crop out over vast areas on the Svalbard archipelago and subcrop under the Barents Sea (Riis et al., 2008). The Middle and Late Triassic has a timespan of 10.2 and 35.7 Ma respectively. A general low resolution of the arctic Triassic is prominent due to the lack of age-diagnostic macrofossils within these deposits. This low resolution is especially true for the Late Triassic stages, which has recently been underlined by Vigran et al. (2014). Four formal zones were established for the Middle and Late Triassic respectively through their work, effectively providing an average resolution of 2.55 Ma for each of the Middle Triassic zones, and 8.9 Ma for the Late Triassic zones. Continued biostratigraphic work is therefore important, especially for the Late Triassic. Subdivision of the formal zones of Vigran et al. (2014) has more recently been performed by Paterson and Mangerud (2015), and signalizes that the biostratigraphic resolution of the Late Triassic is well underway of being improved.

The paralic nature of the Late Triassic successions, as documented by Riis et al. (2008), is an important factor that hampers the obtainment of age diagnostic macrofossils, and further complicates an exact age assignment and biostratigraphic correlation. However, these paralic – deltaic deposits has proven to be favorable for palynology. The rapid evolution and widespread distribution of palynomorphs can thereby aid in improving this resolution, and further reflect upon paleofloral changes and development as a proxy for climate changes through the Triassic period. Additionally, these microfossils are present in most sedimentary types, which allows for interregional correlation between continental and marine environments (Cirilli, 2010).

Triassic strata from the Boreal realm contains proven hydrocarbon source and reservoirs rock intervals, and are of commercial interest (Lundschien et al., 2014). Dating and correlation of these successions is therefore of significant importance for the oil and gas industry. Additionally, the understanding of past climates can be improved with detailed palynostratigraphic research, which is of academic importance.

1.1 Aims of study

This thesis is part of a larger joint industry project entitled ”Middle to Late Triassic palynostratigraphy in the Barents Sea area” currently being undertaken at the University of Bergen. The aim of this larger project is to use palynology to obtain a better stratigraphic resolution through the Upper Triassic since the duration and dating of this period still holds some uncertainties. This study will then work as a contribution to this larger project.

For the purposes of this study, access to the shallow stratigraphic core 7534/4-U-1 was provided by the Norwegian Petroleum Directorate (NPD). The core is drilled in the Sentralbanken area of the Barents Sea, southeast of Svalbard (fig. 1.1). The core has previously been suggested to be of early Carnian age (Julian) by Vigran et al. (2014), and they assigned the assemblage to their *Aulisporites astigmosus* Composite Assemblage Zone. However, no quantitative data or palynofacies analysis was performed. The aim of the present study is to conduct a more detailed analysis to verify the age dating, and determine if the Ladinian – Carnian boundary could be present in this core. Identification and documentation of the present palynomorph assemblages throughout this succession has been conducted by semi-quantitative counts. An additional aim is to integrate the various analysis including palynofacies and core description to provide paleoenvironmental interpretations.

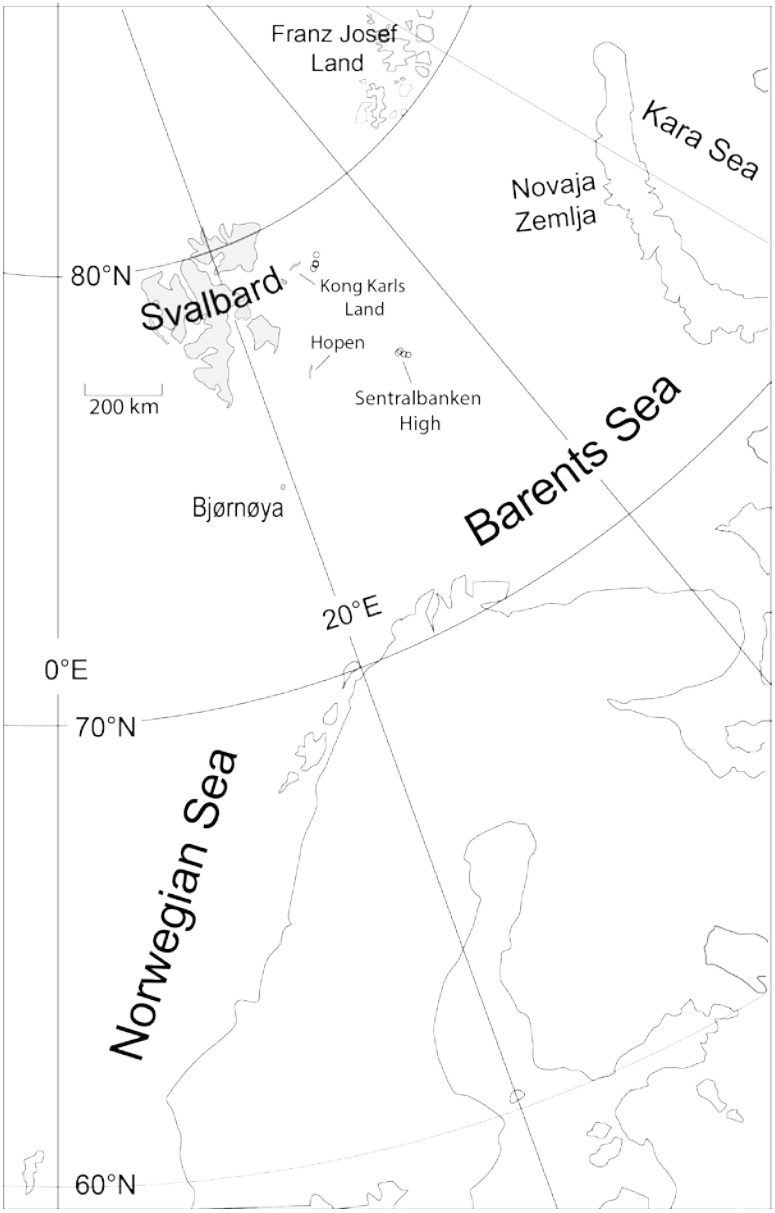

Figure 1.1: Map of the Barents Sea with location of the Sentralbanken High (courtesy of Paterson, N.).

1.2 Palynology

Palynology is defined as the study of organic walled microfossils and comprises plant pollen, spores and certain microscopic plankton organisms (Traverse, 2007). These are collectively termed palynomorphs, and include reproductive particles of plants (e.g. pollen and spores) and whole organisms (e.g. algae) (Traverse, 2007). The walls of these microorganisms are acid resistant, and are composed of either sporopollenin (pollen, certain spores, dinoflagellates and acritarchs) or chitin (spores and fungi), which enables the specimens to be preserved in a maceration preparation with use of hydrochloric acid (HCl) and hydrofluoric acid (HF). The size varies in general from 5-500 µm (most commonly 20-100 µm), and can be of marine or terrestrial origin (Traverse, 2007).

The presence/absence of palynomorphs within sedimentary successions is somewhat dependent on the facies, although one would expect these microfossils in most sedimentary types to a certain extent. Palynomorphs survive long-distance transportation and diagenetic processes due to the robust outer wall of these grains. However, highly alkaline environments or sediment prone to high oxidation will affect the preservation (Traverse, 2007).

Spores include the reproductive bodies of lower vascular plants (club mosses, horsetails and ferns), while pollen represents the sperm-carrying reproductive body of seed plants (gymnosperms and angiosperms). The main distinguishing features between spore- and pollen grains are entirely based on the morphological characteristics.
Spores are characterized by a leasura, a scar located on the exine wall of the grain, occurring as monolete or trilete marks. High abundance of both monolete and trilete spores were recorded from core 7534/4-U-1, e.g. the monolete fern spore *Leschikisporis aduncus* and the trilete spore *Dictyophyllidites mortonii* (Appendix III – plate II and III).
The pollen grains are characterized by a combination of sulcal openings and saccus/saccae. Pollen grains generally have a more complex outer wall and can occur as bisaccates (two saccae), or with one or several sulcal openings. The complex wall structure comprises differently organized collumelae in the exine wall, which can be observed in microscope (using high magnification). This feature causes a wider and a more pronounced

ornamentation of the pollen grains in most cases. Appendix III displays the common pollen taxa recorded in this study, with good examples of bisaccate (e.g. *Alisporites* spp.) and sulcate (e.g. *Chasmatosporites* spp.) genera.

Acritarchs include a wide range of different kinds of organisms, many of which are believed originate from unicellular marine algae (Traverse, 2007). However, the affinity of these microfossils is not known which is reflected by the meaning of the word acritarch; “of uncertain origin” (Traverse, 2007).

These microfossils can be applied as an indicator for composition of present and past biodiversity, for dating and correlation of successions, and as palaeoenvironmental indicators.

1.3 Previous Palynological Work

Numerous palynological studies of Triassic successions has been carried out in the region, both in the subsurface of the Barents Sea (Hochuli et al., 1989; Vigran et al., 1998) and the correlative exposures on Svalbard (Smith, 1974; Smith et al., 1975; Smith, 1982; Bjærke and Manum, 1977; Bjærke, 1977; Bjærke and Dypvik, 1977; Mørk et al., 1990; Vigran et al., 2014; Paterson and Mangerud, 2015).

Smith (1974) studied the Late Triassic Kapp Toscana Group on Hopen, Svalbard, assigning a possible Carnian age for the lowermost strata in southern Hopen (Iversenfjellet) and a Rhaetian age for exposures on northern Hopen near Braastadskardet. Bjærke and Manum (1977) followed up Smith´s work on Hopen, and presented preliminary palynological data from Kong Karls Land followed by a more detailed study by Bjærke (1977). Bjærke and Manum (1977) agreed with Smith´s (1974) age interpretation assigning a Rhaetian age for the exposures on Hopen based on comparisons with Rhaetian assemblages from NW Europe and Arctic Canada. In light of new ammonoid and bivalve evidence from Hopen presented by Korchinskaya (1980), Smith (1982) revised his previous age interpretation and assigned a pre-Rhaetian (Norian) age to the palynological assemblages from the island. Bjærke and Dypvik (1977) conducted a sedimentological and palynological study of the successions of Sassenfjorden on Spitsbergen. The twenty samples collected from this location contained diverse assemblages consisting of pollen, spore, acritarchs and dinoflagellates, and concluded the succession to be of Rhaetian to late Lower Jurassic age (Pliensbachian-Toarcian).

Later, Hochuli et al. (1989) published an informal palynological zonation for the Late Permian to Late Triassic successions on Svalbard and the Barents Sea consisting of 16 assemblages. The assemblages described were based on base and top occurrences of key species (Hochuli et al., 1989). It is important to note that Hochuli et al. (1989) based their work on first downhole appearance, with material mainly collected from well cuttings and did not include any information of sample location. Some of the assemblages were also independently dated by calibrating them to established ammonite zones, and resulted in a more complete record for the Early- and Middle Triassic. The Late Triassic assemblages were based on

correlation of palynomorphs from Germanic and Alpine realms. Vigran et al. (1998) presented biostratigraphic results from the Svalis Dome located in the central Barents Sea including deposits spanning in age from the Lower- to Middle Triassic. Through this study 8 miospore assemblage zones (Svalis-1 to Svalis-8) was established, in which the oldest seven zones spans the Havert, Klappmyss and Steinkobbe formations. Their Svalis-8 assemblage represents the middle part of the Snadd Formation, covering approximately the same succession studied in the current investigation. Vigran et al. (1998) assigned a Ladinian age to this interval based on palynological correlation. Additionally they commented on the established assemblages of Hochuli et al. (1989), and related this to their zones from the Svalis Dome.

The papers mentioned above have been essential for building the framework for the Triassic palynostratigraphy. The recent publication by Vigran et al. (2014) presents a comprehensive review and compilation of previous work including several exploration wells and shallow stratigraphic cores drilled in the Barents Sea, and sections sampled from Svalbard. Through the data gathered they further adjusted and modified the palynozonations by presenting 15 new formal zones for the Triassic Barents Sea. This included four composite assemblage zones established for the Late Triassic, spanning approximately 36 million years, providing a relatively poor resolution (fig. 1.2). This recognition led to the initiation of the larger project of which this current thesis forms a part of. Additionally, a second master project is currently undertaken involving material from Kong Karls Land.

As the first part of this research initiative Paterson and Mangerud (2015) carried out an extensive re-investigation on Hopen, based on the analysis of 156 palynological samples taken from eight localities on the island. The six assemblages described were identified by relative abundance and first stratigraphic appearance, and interpreted to range from late Carnian to Rhaetian age. Paterson and Mangerud (2015) considered their results to be partially correlative with the previous zonations and assemblages established by Hochuli et al. (1989) and Vigran et al. (2014).

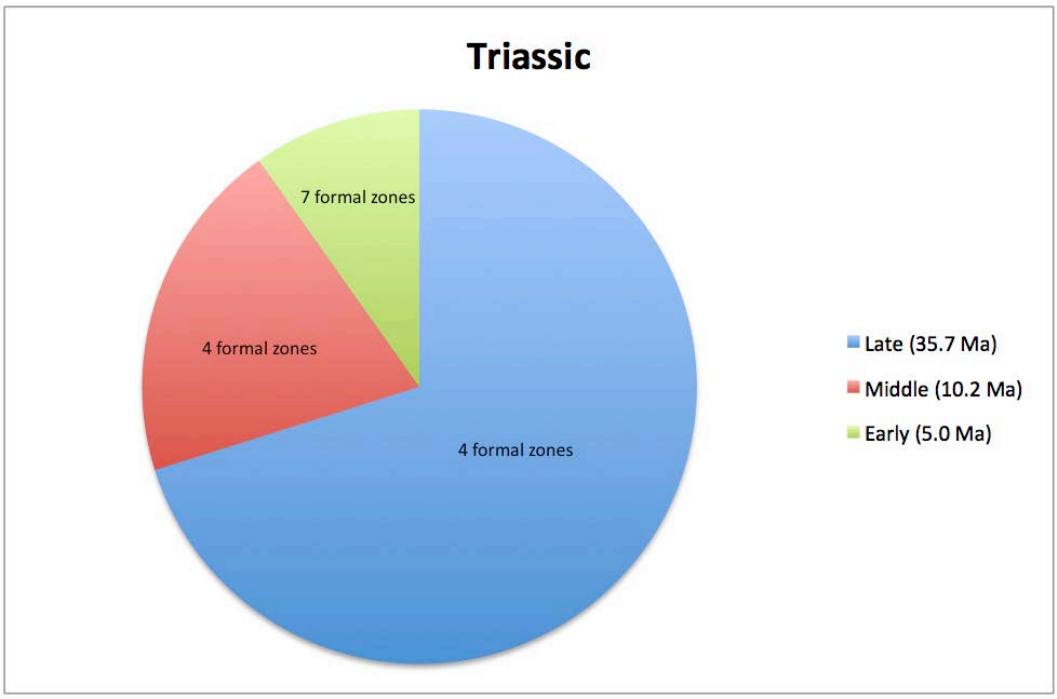

Figure 1.2: The resolution of the Triassic period in the Barents Sea region based on the 15 formal zones defined by Vigran et al. (2014) and calibrated to Boreal ammonite zones. Timespan-estimates based on the ICS-chart v2015.

Previous palynological studies from outside the present Arctic region are quite extensive. The palynology of Triassic successions in the Alpine and Germanic realm has been well documented (e.g. Van Der Eem, 1983; Hochuli and Frank, 2000; Bonis et al., 2009; Kürschner and Herngreen, 2010); however, previous workers in the Barents Sea region have noted significant differences between the compositional features of Alpine and Boreal palynological assemblages (e.g. Hochuli and Vigran, 2010). The various palynological publications are still essential for systematic, palaeoenvironmental and correlation purposes. Important work includes Fisher (1972) who studied the Triassic palynofloral succession in the southwest and midlands of England. Material gathered from surface exposures contained five major assemblages of Lower Triassic (Scythian)-Early Anisian, Ladinian, Early Carnian, Late Carnian, and Rhaetian age. This laid the foundation for further subdivision and zonation of the British Triassic. The succession was also correlated to the Germanic formations. Van Der Eem (1983) observed seven assemblages in the western Dolomites, Italy, with ages corresponding from Upper Anisian to Middle Carnian. Later on, Hochuli and Frank (2000) presented results from their study of the Lower Carnian Raibl Group (also studied by Van Der Eem (1983)) in the Eastern Alps of Switzerland. Six samples from the Cluozza Member (Raibl

Group) were analyzed, and contained assemblages that corresponded to an early Carnian age. Bonis et al. (2009) followed with a more extensive research of the Eiberg Basin in the Northern Alps of Austria, focusing on the Triassic-Jurassic transition. With a total of 66 samples they identified five palynomorph assemblages, and observed a marked change at the Triassic-Jurassic boundary with an increase in spore and pollen diversity (Bonis et al., 2009). The results of these studies were later discussed in Cirilli (2010) in a published review of previous studies focused around the Triassic-Jurassic boundary. Cirilli takes a regional correlative approach by discussing the established palynozonations of the northern and southern hemisphere.

Previous work from the Arctic Canada with a Triassic focus includes Fisher and Bujak (1975), Felix (1975) and Fisher (1979). The latter study presented a Triassic palynofloral zonation of the Canadian Arctic Archipelago, and dated the sections based on material from surface samples, core samples and well cuttings collected from the Arctic islands. The zonations also contain a biostratigraphic control from Triassic ammonite zones previously established by Tozer (1961, 1967) (Fisher, 1979). Nine assemblages were established through this work, assigned to range from Late Induan (Griesbachian) to Rhaetian age, thus covering the whole Triassic period. The similar latitude between the Arctic Canada and the Barents Sea during the Triassic suggests some correlation between these regions, which could be reflected in the palynofloral distribution.

2. Geological Setting: the Late Triassic Barents Sea and Svalbard

Paleogeography

The Barents Sea Shelf, with its central parts located around 75^{o}N 40^{o}E, covers an area of approximately 1.3 million km^{2} (Worsley, 2008). The region can be divided into two main provinces; an eastern region consisting of the large North- and South Barents basins, and a western region characterized by numerous small-scale basins, platforms and structural highs (Worsley, 2008). Triassic strata are subaerially exposed over large areas of the Svalbard Archipelago in the northwestern corner of the Barents Sea, providing an analogue for the successions of the Barents Sea (Lundschien et al., 2014). Most formations and their time-equivalents can be correlated with these exposures (Mørk et al., 1999), where the Triassic successions reach thicknesses of 250-1200 meters (Riis et al., 2008). The region underwent dramatic climate changes as a result of the continuous northward movement of the Eurasian plate (Worsley, 2008). Migration from equatorial latitudes in the Devonian to the present-day high latitudes, led to several tectonic processes along the shelf margins. Worsley (2008) described the late Paleozoic to present-day development of the Barents Shelf in terms of five major depositional episodes. The continental collisions between Baltica and Laurentia (causing the Caledonian Orogeny), and the following collision between Laurasia and Western Siberia (forming the Uralian Mountain chain), are two of the major events that shaped the Barents Sea. These collisions, along with local and regional sea-level fluctuations, played an essential role in the sedimentation of the Barents Shelf (Worsley, 2008). Since this project is aimed at the Middle – Late Triassic development and deposits, the content further discussed will be restricted to this period.

By the end of the Paleozoic Era the Barents Sea had evolved into an embayment with Pangean shorelines to the east, west and south, and with the Panthalassa Ocean located to the north (Riis et al. 2008). Tectonically, the Early and Middle Triassic period is regarded as fairly stable in a paleogeographic sense; however, the massive southern and northern Barents Sea basins were subsiding (Riis et al., 2008). Additionally, the uplift of the Uralian Mountain chain was almost completed by the end of the Permian, forming a major source of sediment to the basin (from the east), which led to the progradation of a vast coastal plain in

a northwest direction (Riis et al., 2008). The subsiding basins of the eastern region became major depocenters for these clastics (Riis et al., 2008). Sediment infill from the south was also prominent, as derived sediment from the Baltic Shield complemented the derivatives from the east. The infill from the southeast during the Triassic is documented by the identification of prograding clinoforms through use of seismic data (Riis et al., 2008; Glørstad-Clark et al., 2010, 2011; Høy and Lundschien, 2011; Lundschien et al., 2014). The extent of the deposits and the progradation of the shoreface are reconstructed by Klausen et al. (2015) at intervals corresponding to their Ladinian – Norian sequences (fig. 2.1), with a furthest reach onto the Svalbard Archipelago in the Late Carnian.

The early Norian represents a marked change in the Barents Sea region. A regional sea-level rise led to a new marine connection between the Tethyan and Boreal oceans. Coastal and shallow marine environments were developed, and extended across the entire Barents Sea Shelf, as illustrated by figure 2.1. The sediment infill from the south-east and subsidence rates of the basin were dramatically reduced due to this transgression.

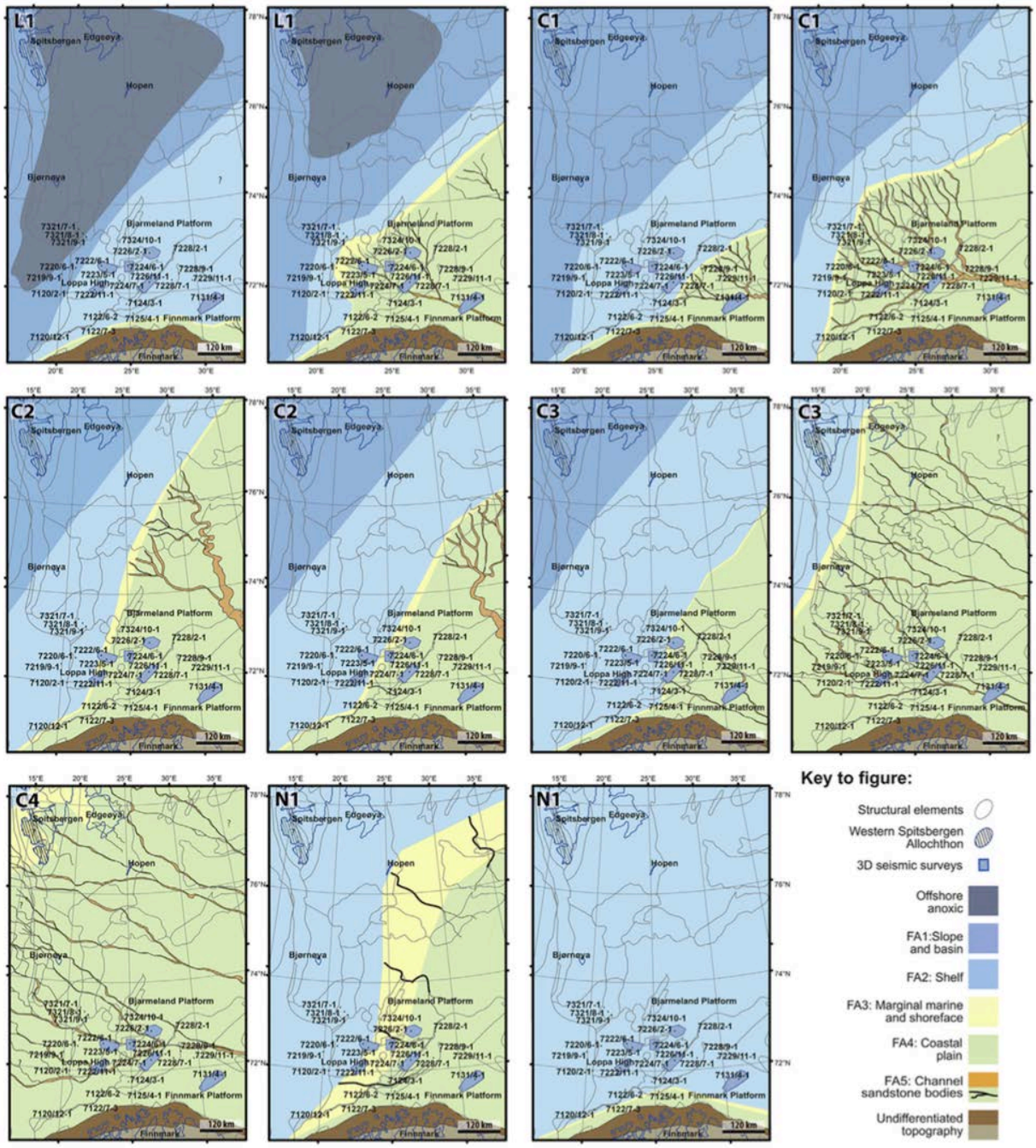

Figure 2.1: Paleogeographic evolution of the south-western Barents Shelf from the Middle to Late Triassic, with progradation from the south-east and extent of the paralic deposits for each sequence. L = Ladinian, C = Carnian, N = Norian (from Klausen et al. (2015)).

Lithostratigraphy

The Triassic to Middle Jurassic of Svalbard is comprised of two main groups first defined by Buchan et al. (1965), with corresponding subgroups, formations and members (fig. 2.2). The Sassendalen Group was later revised by Worsley et al. (1988) to also include the Ingøydjupet Subgroup of the Hammerfest Basin. The group ranges from Early to Middle Triassic (Mørk et al. 1999). The overlying Kapp Toscana Group spans an interval from Late Triassic to Middle Jurassic, and includes the coeval deposits of the Barents Sea Shelf as defined by Mørk et al. (1999).

The Sassendalen Group contains general regional changes in lithology varying from coastal to deltaic deposits on western Spitsbergen, transitioning to shelf mudstones with high content of organic material on the eastern Svalbard and into the Barents Sea Shelf (Mørk et al., 1999). The formations of western Spitsbergen (Vardebukta, Tvillingodden and Bravaisberget formations) are dominantly composed of coastal, deltaic to shallow shelf deposits. These formations correlate with the Vikinghøgda and Botneheia formations of the central and eastern parts of Spitsbergen, and a transition to shelf mudstones (Mørk et al., 1999). The Botneheia Formation contains high abundance of organic material, and is regarded as an important hydrocarbon source rock for the Barents Sea Shelf (Vigran et al., 2014; Lundschien et al., 2014). Further on, in a southeastern direction, the formations of Bjørnøya (Urd Formation), the Svalis Dome (Steinkobbe Formation), and the Hammerfest Basin (Havert, Klappmyss and Kobbe formations), represent deposits of a shallow to deep shelf environment (Mørk et al., 1999). The Steinkobbe Formation of Olenekian to Anisian age is the eastern equivalent of the Botneheia Formation, with high content of organic material, which together with the Botneheia Formation constitutes the most important hydrocarbon source rocks for the region.

As illustrated in figure 2.2, a major transition in the lithofacies occurred at the boundary between the Sassendalen Group and the Kapp Toscana Group. Due to the progressive infill from the southeastern highlands the Snadd Formation initiated the group at an earlier stage (Ladinian) in the Barents Sea compared to the correlative Tschermakfjellet and De Geerdalen formations on Svalbard, which are dated as Carnian. The boundary is thus considered to be

time-transgressive (Riis et al., 2008) and corresponds with the prograding clinoforms from the east, as imaged on seismic by Riis et al. (2008), Glørstad-Clark et al. (2010, 2011), Høy and Lundschien (2011) and Lundschien et al. (2014).

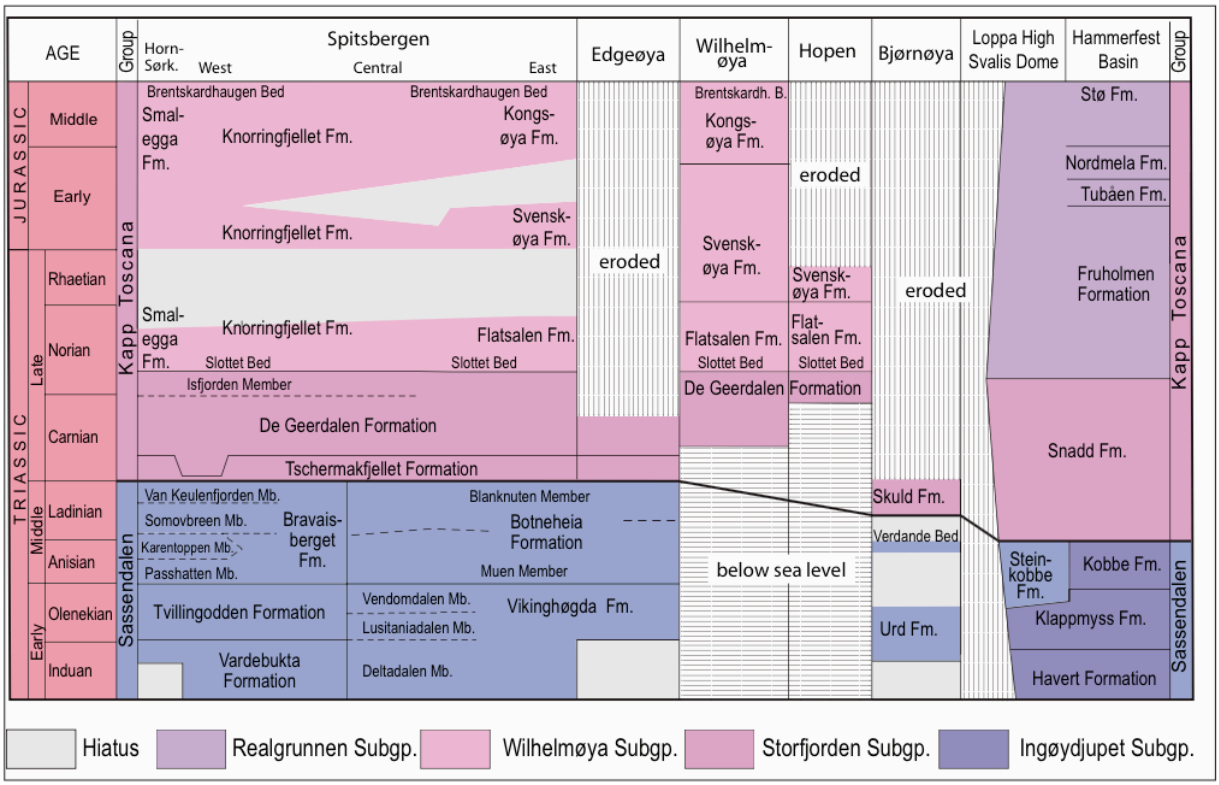

Figure 2.2: Lithostratigraphic subdivision of the Triassic to Middle Jurassic successions of Svalbard and the Barents Shelf. Note the time transgressive boundary between the Sassendalen and Kapp Toscana groups (modified by Lundschien et al., 2014, from Mørk et al., 1999).

The transition into the Kapp Toscana Group is marked by change over to shallow marine to deltaic deposits which in turn has covered the entire Barents Sea Shelf (Mørk et al., 1999). The base of the Kapp Toscana Group on Svalbard consists of grey shales of the Tschermakfjellet Formation coarsening upwards into sandstones of the De Geerdalen Formation. They range in age from early Late Triassic (Carnian) to the Middle Jurassic (Bathonian), and are present throughout the Barents Sea Shelf, with exposures on Spitsbergen, Barentsøya, Edgeøya, Hopen, Kong Karls Land and Bjørnøya (Mørk et al., 1999). The Kapp Toscana Group has been further divided into three subgroups (Mørk et al., 1999) based on stratigraphic differences. Mudstones and sandstones of the Tschermakfjellet and

De Geerdalen formations deposited on Spitsbergen and the eastern islands dominate the lowermost unit, the Storfjorden Subgroup. The sand-rich subgroup continues eastward on Bjørnøya with the Skuld Formation, and further on, to the Svalis Dome and Hammerfest Basin with the Snadd Formation.

The Wilhelmøya Subgroup includes the successions exposed on Spitsbergen, Wilhelmøya and Hopen. The five formations within this unit are characterized by mature sandstones related to deltaic through shallow marine environments, and with a depositional age of Norian to Bathonian (Mørk et al., 1999).
The Realgrunnen Subgroup forms the equivalent unit of the Wilhelmøya Subgroup on the Barents Sea Shelf. It is subdivided into four formations, with the lowermost, the Fruholmen Formation constituting the Late Triassic succession, showing very similar lithological properties. A transgression during the early Norian led to development of deltaic systems, prompting the deposition of these sand-rich successions throughout the rest of the Late Triassic. Consequently, the initiation of the Fruholmen Formation is characterized by prominent shale intervals in the earliest stage, punctuated by minor interbeds of coal, and a further upward grading into mature sandstones (Mørk et al., 1999).

The depositional setting of the Kapp Toscana Group, formed by the evolving paralic platform during the Middle and Late Triassic, has resulted in the formation of sandstone rich intervals of the Snadd Formation representing potential hydrocarbon reservoir rocks as well as close lying organic rich shales representing potential source rocks of the Botneheia Formation.

3. Materials and Methods

3.1 Samples

The shallow stratigraphic core 7534/4-U-1 covers a length of 233 meters, and was provided to this project by the Norwegian Petroleum Directorate (NPD). The core was drilled in the Sentralbanken area of the Barents Sea, southeast of Svalbard in 1995 by SINTEF (contracted by the NPD) (Riis et al., 2008). A total of 56 samples were extracted from the core (fig. 3.1), with 31 of the slides from the NPD collection (processed by SINTEF), and the remaining 25 samples taken in 2013 (table 4.1). The combining of these two sets provided an approximate resolution of one sample per 4 m. The set of slides includes both un-oxidized samples for palynofacies analysis and oxidized samples for palynological analysis. A second oxidation of miscellaneous samples was carried out to improve the preservation, and proved helpful in most cases. The preservation of the samples was highly variable throughout the core. No samples were totally barren, however a significant amount was very poorly preserved. Complete counts were performed for the moderately to well-preserved samples, and the poorest samples were only scanned for present species and genera (see Appendix II).

The core was described during a week at NPD in 2014 (see fig. 4.6). Since the main scope of this thesis is palynology a detailed sedimentological analysis was not performed.

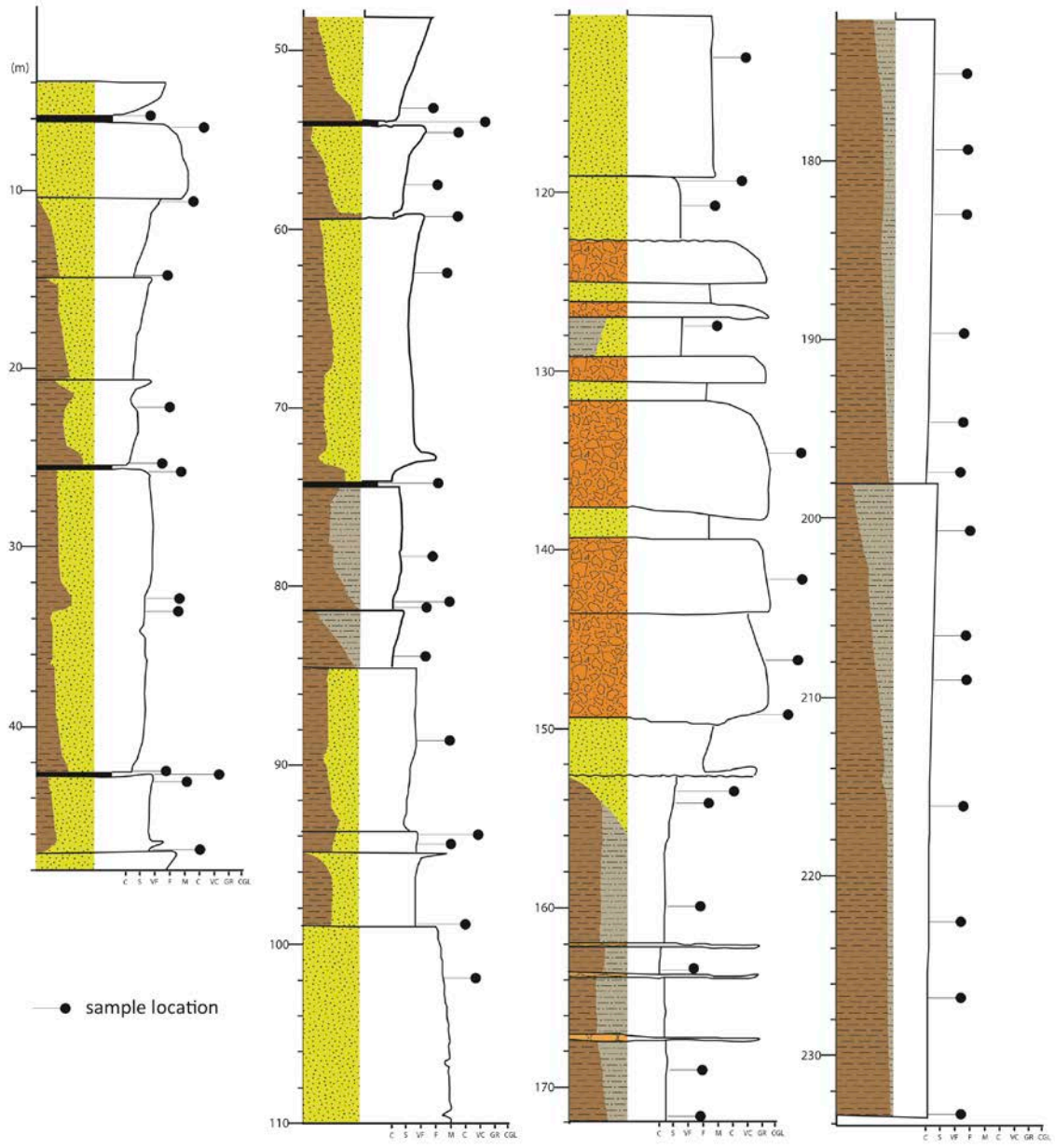

Figure 3.1: Simplified log of core 7534/4-U-1 with corresponding sample locations.

3.2 Preparation

The prepared slides from the core 7534/4-U-1 were processed by applying palynological preparation techniques (fig. 3.2). After the initial sampling of the material the following steps involve crushing, drying and weighing of the material. The preparation technique continues with carbonate removal, by adding hydrochloric acid (HCl), and silicate removal, by adding hydrofluoric acid (HF) in the order as listed. The hydrochloric acid is performed first to remove all Ca^{+} ions, which could form calcium fluoride on reaction with HF-acid. Neutralization of the acids is conducted after both these steps by adding distilled water, followed by sieving at preferably 6-14 microns. If any fluorosilicates has formed through reaction with the HF-acid, a last step is conducted by adding another round with hydrochloric acid. The final steps involve sieving, oxidation and ultrasound. The set of samples provided contained both oxidized and un-oxidized material, where the un-oxidized samples were used for palynofacies analysis. The oxidation is normally conducted by the use of nitric acid (HNO_3) with purpose to remove unwanted organic material and obtain cleaner slides better suited for palynological analysis. Final centrifuging is performed to separate and remove heavy minerals from the samples. Diluted hydrochloric acid (HCl) or phenol is often added to the microscope slides when mounted to prevent fungal growth.

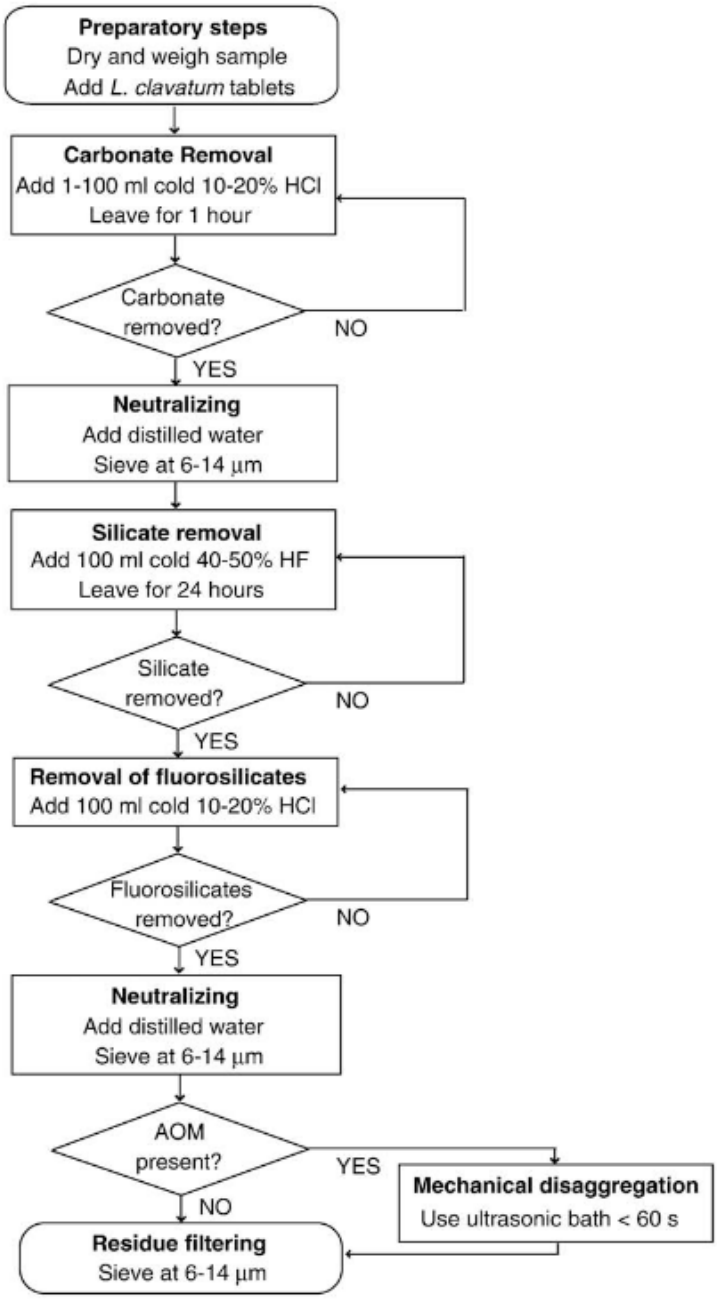

Figure 3.2: Flow chart of the standard palynological preparation technique. AOM = amorphous organic matter (from Mertens et al., 2009).

3.3 Quantitative palynology

The samples were analyzed using a Zeiss Axioplan microscope, and 200 specimens were counted for most of the slides. Additionally, all slides were scanned for species that were present outside of the count and was recorded as present in the range chart (marked with a "+"-sign)(Appendix II). This additional "scan" was important to conduct in order to detect the less dominant/rarer taxa (e.g. certain acritarchs and algae). 21 samples were not counted, due to low palynomorph recovery. The species identified throughout this analysis include spores, pollen grains, acritarchs and algae. Pictures of selected palynomorphs were taken with a Zeiss-Axio Imager.A2 AxioCam ERc 5s (Appendix III).

The original descriptions given by Bjærke and Manum (1977) and Klaus (1960) provided relevant taxonomic information used for determination of various species and genera. Even though the descriptions of Klaus (1960) are given in German, it also contained good quality plates of important taxa. The paper by Pautsch (1973) also proved helpful, containing descriptive information of certain pollen and spores, also including excellent plates. In addition to the original descriptions of taxa, papers including Vigran et al. (2014) and Paterson and Mangerud (2015) have been of great importance in getting familiar with the assemblages and various species.

The quantitative data was entered in Stratabugs in order to produce good quality range charts of the palynological results (Appendix II). Due to the varying preservation of the material, the identification of the taxa alternated between genus level and species level. The preservational differences also caused some of the identifications to remain uncertain/questionable. These individual counts have been marked with a question mark in the range chart (Appendix II).

3.4 Palynofacies analysis

This analysis required study of the un-oxidized samples (56 in total), which was taken at the same intervals as the ones used for quantitative palynology. Microscopy was carried out using the same microscope as for the quantitative palynology analysis, primarily in 20x objective. The methodology encompasses visual volume estimates of the organic material present in each slide. Identification of the particulate organic matter (POM) involved observations in 10 fields of view, and further calculation of average value of each constituent. To obtain representative results the analysis was conducted by observing the middle parts of the slides, to avoid areas with density differences which often appears near the margins of a palynological slide.

Palynofacies is the study of sedimentary organic matter and the term was first applied by Combaz (1964). The organic material relates to the depositional environment in much the same way as different types of sediments (angularity/grain-size/sorting). These observations may be applied to determine transport distance and interpretation of the paleoenvironment. Several classifications of the organic matter have been proposed, but Tyson (1995) gives the more accurate and complete classification scheme. Thus, the analysis has been carried out using the classification developed by Tyson (1995)(modified in table 3.1).

The main categories are separated in four main units: zooclasts, palynomorphs, phytoclasts and amorphous organic matter ("AOM")(table 3.1). Identification of the present material was recorded by the amounts of these individual units.

The initial step is to identify if the organic matter has structured or structureless features. The amorphous group comprises the structureless material; occurs in varying shapes without any clear outlines (fig. 4.7). AOM can be marine or terrestrial in origin; marine AOM originates from phytoplankton- or bacterially-derived material, while terrestrial AOM comprises amorphous products of plant resins and macrophyte tissues (Tyson, 1995). It is characterized by a pale to brown-yellow color, and commonly dominates in sediments deposited in anoxic marine environments, with low input of terrestrially derived organic matter (Tyson, 1995).

The structured material comprises the phytoclasts group, zooclast group and the palynomorph group. Both zooclasts and phytoclasts occur as fragmentary particles, and are further distinguished by the animalian features of the zooclasts (e.g. spines, hairs, joints) and the non-animalian particles of the phytoclasts (e.g. leaf cuticles, cortex tissue, wood, bark).

Table 3.1: Classification of sedimentary organic matter used for palynofacies analysis (modified from Tyson (1995)).

	Category	Source	Constituent
Structured	Zooclasts	Zooplankton and Zoobenthos	Graptolite debris Arthropod debris
	Palynomorphs	Zoomorphs	Scolecodonts Tectin foraminiferal linings Chitinozoa
		Organic-walled Phytoplankton (including meroplankton)	Prasinophyte phycomata
			Chroococcale cyanobacteria
			Chlorococcales: Botryococcates Hydrodictyales
			Dinocysts Acritarchs Rhodophyte spores
		Sporomorphs	Miospores: microspores pollen Megaspores
	Phytoclasts	Macrophyte plant debris	Cuticle/epidermal tissue
			Cortex tissue
			Secondary xylem (wood)
			Charcoal Biochemically oxidized wood
		Fungal debris	Hyphae
Structureless	Amorphous ("AOM")	Higher plant secretions	Intra-/extra-cellular resins
		Flocs	Organic aggregates and Faecal pellets
		Phytoplankton	
		Bacteria	Cyanobacteria/Thiobacteria
		Higher plant decomposition products	Humic cell-filling precipitates Humic extracellular precipitates

Cuticle fragments constitutes the outermost waxy covering of leaves and stems of most plants (Tyson, 1995). The fragments are characterized by its unaltered cellular texture and thin pale yellow to light brown color (fig. 4.7).

Woody tissue or coaly material is observed as fragments with cellular structure, often occurring as “xylem elements” (plant stem)(fig. 4.7e), with pitting or spiral thickenings (Tyson, 1995). These particles are generally very common, but increase with proximity to the source, especially in proximal delta zones.

“Gelified wood” (from Tyson, 1995) constitutes opaque particles with sharp angular outlines mostly observed without any definite biostructure. It is recognized by a dark color with translucent margins (distinct from charcoal), and a conchoidal fracture (Tyson, 1995)(fig. 4.7). The sharp-edged textures and color of these fragments are believed to represent the effect of oxygenation, erosion and reworking (Tyson, 1995).

The palynomorph group is comprised of pollen, spores, acritarchs and dinoflagellates among others. These organic walled microfossils tend to settle in finer sediments and will be more common in the silt/clay size-fraction. As the quantitative palynology has provided detailed information of the different palynomorphs present throughout the core, no distinction has been done in the palynofacies analysis.

A distinction between true AOM and other degraded structureless phytoclasts can often be difficult. However, classifying these is possible with the use of microscopes with UV-fluorescence. Such microscopes were not available for this study, which made this distinction impossible.

4. Results (Shallow Stratigraphic Core 7534/4-U-1)

4.1 Quantitative Palynology

A basic overview of each sample is given in table 4.1, including information of the sampled lithology. The newer sample set is marked with “2013” (table 4.1), and were included to improve the sample density throughout the whole succession. The poorest samples includes 5.97 m, 42.32 m, 42.70 m, 57.57 m, 112.32 m, 120.65 m, 134.57 m and 200.74 m.

A strong terrestrial signature was observed throughout, as the main constituents within the recorded assemblages include fern, lycopsid and bryophyte spores, and conifer and cycad pollen. Spores dominated in the upper part of the core (from 152.80 m to 4 m)(fig. 4.1), while pollen dominated in the lower part (below 152.80 m). An acme of the fern spore *Leschikisporis aduncus* was observed from the sample at 25.63 m taken in a coal bed. Additionally there was also recorded a significant increase in the lycopsid spore *Krauselisporites* spp. in the sample from 83.97 m. These two acmes represent the most prominent changes observed through this core. Due to very poorly preserved samples, no counts were done in the interval between 101.80 m to 149.15 m. However, all these samples contained high abundances of plant fragments. Heavily pyritized samples were also encountered, which often complicated classification to species level. An increase in marine acritarchs was observed in the lower, otherwise pollen dominated interval, in the 17 analyzed samples between 234 m and 152.80 m. Acritarchs were also observed sporadically from 101.80 m up to 22.05 m, however in very low numbers.

On the basis of the quantitative changes observed through the core, a division into three assemblages has been conducted. These assemblages are described in detail below. The reader is referred to the range chart for a detailed overview of each assemblage (Appendix II).

Table 4.1: Complete list of samples from core 7534/4-U-1.

Sample	Sample depth	Sampled lithology	Preservation	Sample set (from)	
#56	**5,97m**	Dark, organic rich mudrock	Very poor	NPD	Assemblage SB-III
#55	**6,24m**	Grey mudrock with small plant fragments	Moderate	NPD	
#54	**10,53m**	Grey siltstone with plant fragments	Poor	2013	
#53	**14,82m**	Intercalated mud and siltstone, bioturbated	Moderate	NPD	
#52	**22,05m**	Grey siltstone, laminated	Moderate-Good	NPD	
#51	**25,63m**	Black vitreous coal	Good	2013	
#50	**25,71m**	Grey seat earth, with plant fragments	Poor-Moderate	2013	
#49	**32,77m**	Dark, organic rich mudrock	Moderate-Good	NPD	
#48	**33,60m**	Dark grey, laminated, fissile mudrock	Good	NPD	
#47	**42,32m**	Grey, laminated mudrock	Very poor	NPD	
#46	**42,49m**	Intercalated mud and siltstone, bioturbated	Moderate-Good	NPD	
#45	**42,70m**	Coal/seat earth	Very poor	NPD	
#44	**46,94m**	Grey siltstone/ Seat earth	Poor-Moderate	2013	
#43	**53,27m**	Dark grey, laminated mudrock	Good	NPD	
#42	**54,09m**	Coal	Moderate	NPD	
#41	**54,23m**	Siltstone with coal	Good	2013	
#40	**57,57m**	Intercalated mud and siltstone, with plant frag.	Poor	2013	
#39	**59,33m**	Dark, organic rich mudrock	Moderate	2013	
#38	**62,26m**	Grey siltstone and sandstone, bioturbated	Moderate-Good	NPD	Assemblage SB-II
#37	**74,11m**	Dark, organic rich mudrock	Poor	NPD	
#36	**78,22m**	Grey mudrock with small plant fragments	Moderate	2013	
#35	**80,90m**	Black, fissile mudrock, with pyrite	Moderate-Good	2013	
#34	**81,28m**	Coal/seat earth	Moderate	2013	
#33	**83,97m**	Dark, organic rich mudrock	Moderate-Good	NPD	
#32	**88,43m**	Seat earth: grey brown with plant frag.	Moderate	2013	
#31	**93,90m**	Black laminated mudrock	Poor-Moderate	2013	
#30	**94,29m**	Laminated, intercalated silt and mudstone	Moderate-Good	NPD	
#29	**98,94m**	Grey siltstone and sandstone	Poor-Moderate	NPD	?
#28	**101,80m**	Thin grey mudrock with plant frag.	Poor	2013	
#27	**112,32m**	Finely laminated siltstone, coal debris	Very poor	NPD	
#26	**119,31m**	Thin grey mudrock with plant frag.	poor	2013	
#25	**120,65m**	Thin grey silstone, with plant frag.	Very poor	2013	
#24	**127,53m**	Grey siltstone, laminated	Poor-Moderate	NPD	
#23	**134,57m**	Finely laminated siltstone	Very poor	2013	
#22	**141,74m**	Intraformational conglomerate	Poor-Moderate	NPD	
#21	**146,06m**	Grey siltstone, cross laminated with sandstone	Poor	2013	
#20	**149,15m**	Grey siltstone and sandstone, with plant frag.	Poor-Moderate	2013	
#19	**153,55m**	Laminated, intercalated silt and mudstone	Moderate	2013	Assemblage SB-I
#18	**154,17m**	Laminated, intercalated silt and mudstone	Poor-Moderate	NPD	
#17	**159,90m**	Grey, fissile mudrock	Moderate	2013	
#16	**163,48m**	Laminated, intercalated silt and mudstone	Good	NPD	
#15	**169,0m**	Finely laminated, fissile mudrock	Moderate-Good	2013	
#14	**171,83m**	Laminated, intercalated silt and mudstone	Good	NPD	
#13	**175,10m**	Dark grey, laminated mudrock	Good	NPD	
#12	**179,33m**	Dark grey, laminated, fissile mudrock	Good	NPD	
#11	**183,02m**	Dark grey, laminated, fissile mudrock	Moderate-Good	2013	
#10	**189,66m**	Black, fissile mudrock, with pyrite	Moderate-Good	NPD	
#9	**194,53m**	Black laminated mudrock	Moderate	NPD	
#8	**197,38m**	Black, fissile mudrock, with pyrite	Moderate-Good	NPD	
#7	**200,74m**	Light grey siltstone, with plant frag.	Poor	2013	
#6	**206,53m**	Laminated silt and mudstone	Moderate-Good	NPD	
#5	**209,06m**	Grey, laminated mudrock	Moderate	2013	
#4	**216,09m**	Dark grey, laminated mudrock	Moderate-Good	NPD	
#3	**222,44m**	Black, laminated, fissile mudrock	Good	2013	
#2	**226,72m**	Black, laminated, fissile mudrock	Moderate	NPD	
#1	**233,48m**	Black, laminated, fissile mudrock	Moderate-Good	NPD	

Assemblage SB-I (233.48 - 153.55 m) (#1 - #19)

This assemblage covers the interval between 153.55m to 233.48m, including the lowermost part of core 7534/4-U-1. The samples analyzed from this interval were generally well preserved, with the exception of one sample from 200.74m (table 4.1). The assemblage is dominated by bisaccate pollen, in addition to common amounts (≈ 10%) of the monolete fern spore *Leschikisporis aduncus*. *Triadispora* spp. has its highest abundance in this interval, along with *Alisporites* spp., *Angustisulcites klausii* and indeterminate bisaccate pollen grains. Additionally, the striate pollen grain *Stratoabieites balmei* has a consistent occurrence. Several long-ranging taxa also occur in relatively common amounts, including: *Calamospora tener, Deltoidospora* spp., *Illinites chitinoides* and *Araucariacites australis* (Appendix II).

The recorded spora taxa include *Aratrisporites* spp., *A. laevigatus, A. scabratus, Apiculatisporis parvispinosus, Baculatisporites* spp., *Calamospora tener, Camarozonosporites rudis, Conbaculatisporites* spp., *C. hopensis, Deltoidospora* spp., *Dictyophyllidites mortonii, Krauselisporites* spp., *K. cooksonae, Kyrtomisporis laevigatus, Leschikisporis aduncus, Limatulasporites limatulus, Porcellspora longdonensis, Punctatisporites* spp., *Striatella seebergensis and Thomsonisporites toralis.*

Recorded pollen taxa: *Alisporites* spp., *Angustisulcites klausii, Araucariacites australis, "Bisaccate* spp." (indet.), *Chasmatosporites* spp., *C. hians, C. apertus, Cycadopites* spp., *Echinitosporites iliacoides, Illinites chitinoides, Lunatisporites* spp., *Ovalipollis* spp., *O. pseudoalatus, Protodiploxypinus* spp., *P. ornatus, Podosporites amicus, Schizaeoisporites worsleyi, Staurosaccites quadrifidus, Striatoabieites* spp., *S. balmei, S. multistriatus, Triadispora* spp., *T. verrucata, T. obscura* and *Vitreisporites pallidus*.

This assemblage contains the highest abundance of marine taxa in this core. The marine acritarch *Michrystridium* spp. was the most common taxon, with records of 10.5 % in the sample from 226.72m and 10 % in the sample from 197.38m. *Veryhachium* spp. were also recorded, however in a more sporadic manner. *Cymatiosphaera* spp. were abundant in sample 197.38m.

Unassigned interval (149.15 – 98.94 m) (#20 - #29)

Table 4.1 displays poorly preserved samples within this interval. No complete assemblage could be obtained from these samples. Comparing this part of the succession to the underlying or overlying assemblages was thereby impossible, and led to this unassigned gap in core 7534/4-U-1.

Assemblage SB-II (94.29 – 62.26 m) (#30 - #38)

This assemblage differs from the underlying Assemblage SB-I by a marked increase in monolete, cavate spore *Aratrisporites* spp, including species *A. laevigatus* and *A. scabratus*. A significant abundance peak of the cavate trilete spore *Krauselisporites* spp. is recorded in sample 83.97m (Appendix II). Additional features include a marked reduction of *Triadispora* spp., *Striatoabieites balmei* and *Alisporites* spp. A marked decrease, compared to the assemblages below, in both taeniate and non-taeniate bisaccate pollen is prominent in this spore-dominated assemblage. Marine acritarchs are present in very low numbers and poor consistency, as opposed to the underlying Assemblage SB-I.

The recorded spore taxa of dominant to common abundance include *Aratrisporites* spp., *A. scabratus, Calamospora tener, Conbaculatisporites* spp., *Deltoidospora* spp., *Dictyophyllidites mortonii, Krauselisporites* spp., *Krauselisporites cooksonae* and *Leschikisporis aduncus.*

Other rare to very rare presence of spores include *Annulispora folliculosa, Anapiculatisporites spiniger, Apiculatisporis parvispinosus, Aratrisporites laevigatus, Baculatisporites* spp., *Camarozonosporites rudis, Conbaculatisporites hopensis, Duplexisporites problematicus, Podosporites amicus, Punctatisporites* spp., *Striatella parva, S. seebergensis, Thomsonisporites toralis* and *Zebrasporites interscriptus.*

The dominant to common pollen include *Araucariacites australis, "Bisaccate"* spp. (indet.), *Chasmatosporites* spp., *C. hians* and *Illinites chitinoides.*

Other pollen taxa with rare occurrences include *Alisporites* spp., *Aulisporites astigmosus, Angustisulcites klausii, Chasmatosporites apertus, Cycadopites* spp., *Echinitosporites iliacoides, Lunatisporites* spp., *Ovalipollis* spp., *Protodiploxypinus* spp., *P. ornatus, Ricciisporites umbonatus, Staurosaccites quadrifidus, Striatoabieites* spp., *S. balmei, Triadispora* spp., *Vesicaspora fuscus* and *Vitreisporites pallidus.*

Michrystridium spp. and *Veryhachium* spp. were recorded in very low numbers and had only sporadic occurrences.

Assemblage SB-III (59.33 – 5.97 m) (#39 - #56)

Most of the same taxa that were recorded in assemblage SB-II are also recorded in this uppermost assemblage of core 7534/4-U-1. However, a significant change in the abundances of various taxa differentiates it from Assemblage SB-II. A marked increase in the monolete fern spore *Leschikisporis aduncus* is recorded, dominating the assemblages in most samples within this interval. This is especially true for sample 25.63m, where this single species accounts for 55% of the present palynomorphs, representing the most characteristic feature of Assemblage SB-III (Appendix II). Additionally, a marked decrease in the *Aratrisporites* and *Krauselisporites* genera is recorded compared to the assemblage below. Marine acritarchs continue to have rare and sporadic occurrences, in a similar pattern as observed in Assemblage SB-II.

The common and dominant occurrences of spore taxa recorded within this assemblage include *Leschikisporis aduncus, Deltoidospora* spp., *Dictyophyllidites mortnii, Apiculatisporites parvispinosus, Krauselisporites* spp., *Striatella seebergensis, Calamospora tener, Aratrisporites* spp. and *Conbaculatisporites hopensis*.
Rare occurrences include *Aratrisporites macrocavatus, Aratrisporites scabratus, Krauselisporites cooksonae, Striatella parva, Baculatisporites* spp. and *Anapiculatisporites spiniger.*

Common occurrences of pollen taxa include *Araucariacites australis, Chasmatosporites* spp.*, Chasmatosporites hians, Chasmatosporites apertus, Podosporites amicus, Ovalipollis* spp.*, Cycadopites* spp. and *Illinites chitinoides.*

Rare and sporadically occurring pollen include *Echinitosporites iliacoides, Ricciisporites umbonatus, Triadispora* spp.*, Protodiploxypinus* spp. and *Alisporites* spp.

Marine acritarchs were recorded in the samples at 22.05 m, 25.71 m, 32.77 m, 33.60 m, 46.94 m, 53.27 m and 54.23 m, however in very low amounts. The species present include *Michrystridium* spp. and *Veryhachium* spp.. Additionally, *Cymatiosphaera* spp. were recorded in sample 54.23m.

4.2 Core Description

The Sentralbanken core was divided into four separate sedimentological units (A-D) based on the interpretation of depositional environment. The main features of each unit are illustrated in figure 4.2-4.5. Since the sedimentological part is of secondary focus the different facies has been commented collectively for each unit. The respective units are listed in table 4.2, followed by a more detailed review below. Sedimentological characteristics separate each unit by differences in lithology, color, grain size, rounding and sedimentary structures, along with varying degree of bioturbation and presence/absence of bivalves and shell fragments. In some cases the units are separated by marked erosional boundaries. A log of core 7534/4-U-1 is presented in figure 4.1, with marked boundaries between each unit.

Table 4.2: List of facies associated units from core 7534/4-U-1.

Facies association	Main features	Interval	Interpretation
D	Upward coarsening sequences grading from silty shales to sandstones, capped with coal	99 m – 4 m	Interdistributary bay
C	Sandstone with ripple cross-lamination and cross-stratification	119.05 m – 99 m	Delta sand flat
B	Intraformational conglomerate with sandstone matrix and ripup-clasts of mudstone and siltstone	152.80 m – 119.05 m	Channel system
A	Laminated mudstone coarsening upwards into muddy siltstone	233.60 m – 152.80 m	Open marine, Pro-delta

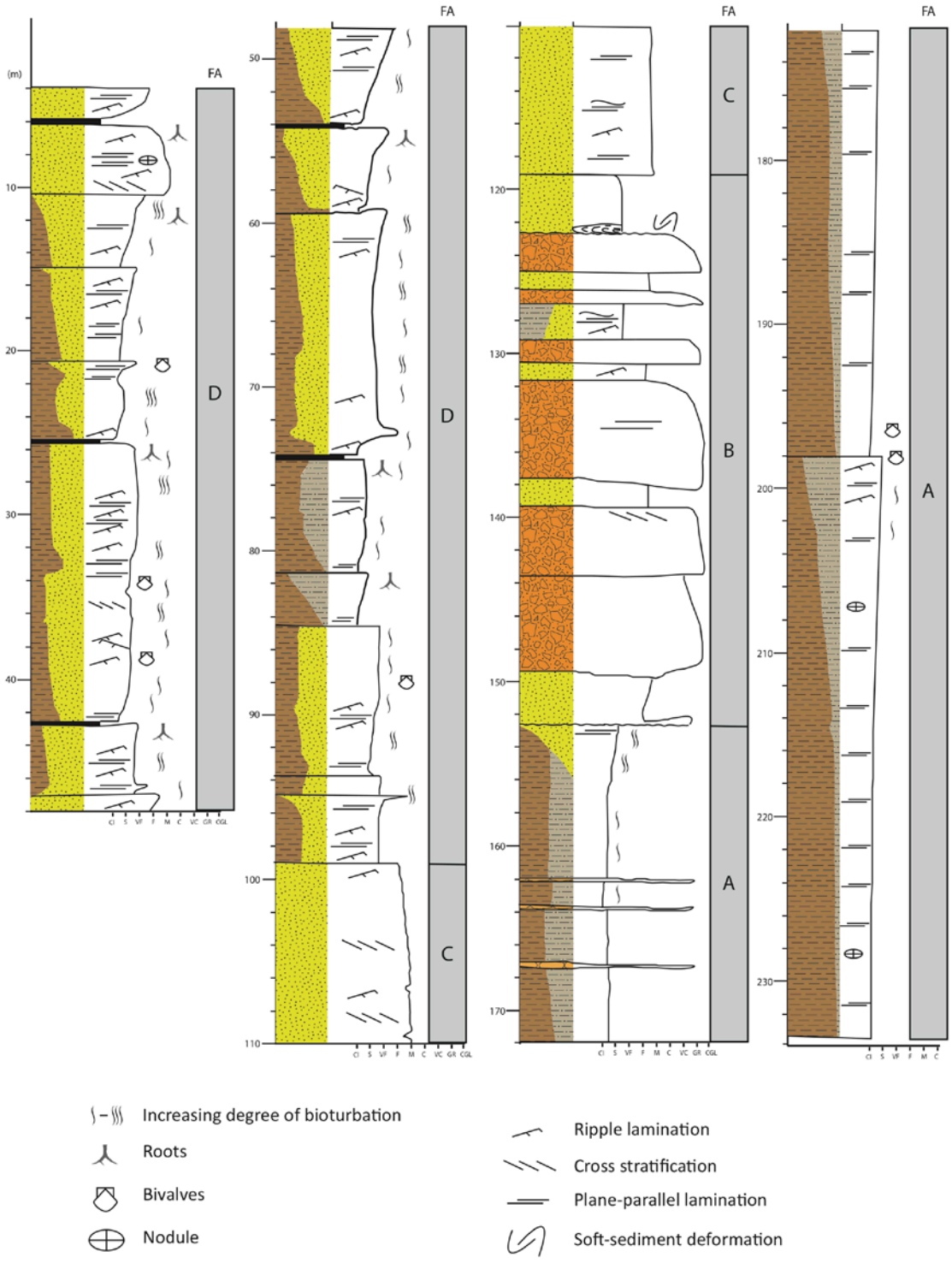

Figure 4.1: Log of core 7534/4-U-1. Divided facies associations (FA) are displayed, in addition to lithological variations. The structural elements are illustrated in a legend (bottom).

Unit A comprises the lowermost unit stretching from 233.50 m to 152.80 m (fig. 4.1). This unit is characterized by two main upward coarsening sub-units of shale (fig. 4.2b) with increasing silt content and a gradual transition upwards into siltstone with minor mud content (fig. 4.2a). Ripple cross-lamination was observed in the top of some sub units (fig. 4.1). Bioturbation is very sparse in the lower part, but increases towards the top of the unit. Bivalves were observed, along with pyrite nodules and siderite beds. Gravel conglomerates were recorded in three thinbeds of 2-3 cm each, at 162 m, 163.80 m and 167.70 m respectively (fig. 4.2c).

Figure 4.2: Main lithologies and boundaries of unit A. Siltstone with mud lamination (a), finely laminated dark mudstone (b). Gravel conglomerate thinbeds (c).

Unit B spans about 30 meters between 152.80 m and 119.05 m (fig. 4.1). Its base is marked by an erosional boundary (at 152.80 m)(fig. 4.3c), overlain by a relatively uniform sandstone bed. The unit represents a significant change in lithology compared to the underlying unit, and is characterized by chaotic beds of conglomerates (fig. 4.3a) fining upwards into fine-medium sandstones. The conglomerates are composed of a fine to medium sized sand matrix, and angular rip-up clasts of mainly siltstone and mudstone, in what seems to be matrix supported. One can observe soft-sediment deformation within these clasts (partly visible in lower fig. 4.3a), which has been ripped up from the underlying Unit A. The sandstone beds change from the more massive beds in the lower parts to more ripple cross-laminated and cross-stratified in the upper parts. No bioturbation was observed in this unit. Organic bands were recorded sporadically throughout the interval.

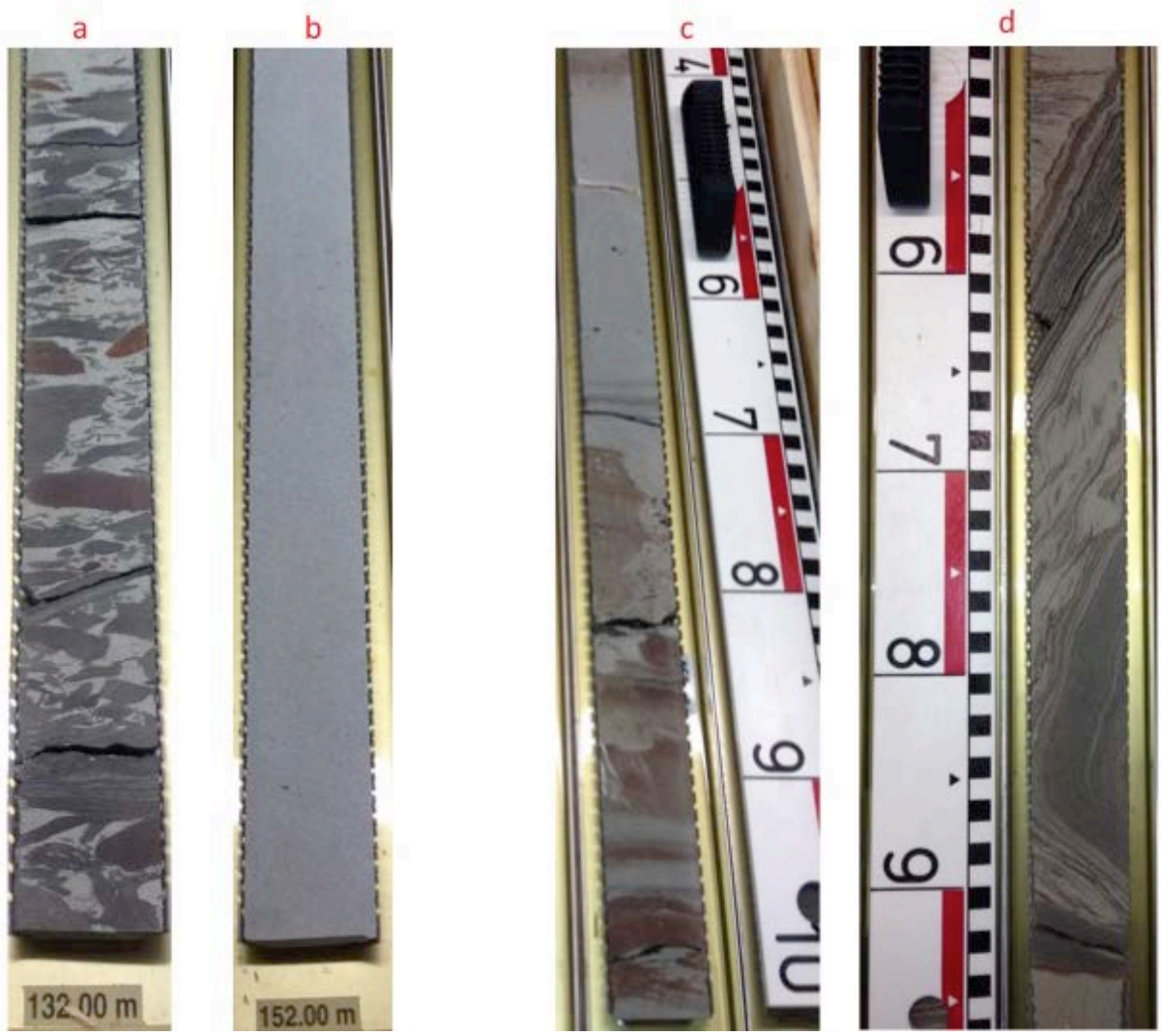

Figure 4.3: Main lithologies and boundaries of unit B. Intraformational conglomerate (a), massive sandstone beds (b). Erosional surface boundary at 152.80 m (c), soft sediment deformation (d).

Unit C spans the interval between 119.05 m and 99 m (fig. 4.1). Heterolithic deposits with flaser bedded medium grained sandstone characterize this unit, along with thin interlayers of organic debris. Internal structures vary between smaller scale ripple laminations in the lower part (fig. 4.4a, b) and low-angle cross stratification in the upper parts (fig. 4.4c). No bioturbation was observed in this unit. Thin siderite beds were recorded throughout this interval (red beds in fig. 4.4c).

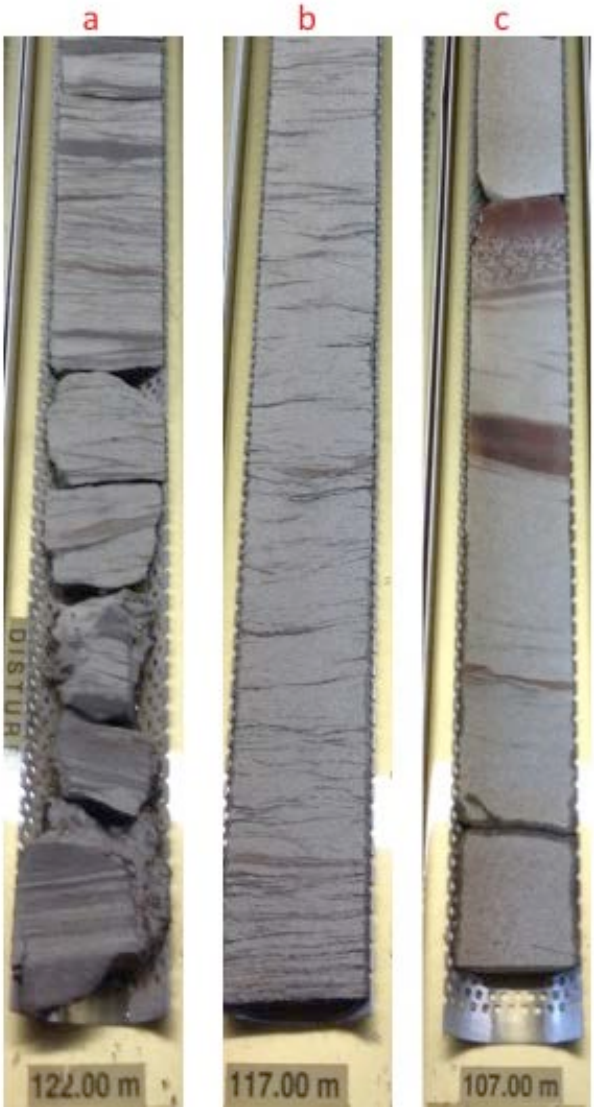

Figure 4.4: Main lithologies of unit C. Flaser bedding and small-scale ripple cross-lamiation (a, b), low angle cross-stratified sandstone with siderite beds (c).

Unit D is the uppermost unit and covers the remaining core interval between 99 m and 4 m (fig. 4.1). The transition from unit C is marked by a clear lithological change, going from medium grained sandstone (unit C) to very fine sandstone and siltstone alternating between lenticular and wavy bedding (unit D). Each sequence is capped with grey seat-earth with roots (paleosol) (fig.4.5a, b) and coal, and is comprised of several parasequences, with a general coarsening upwards trend. This interval comprises the highest degree of bioturbation observed in this core, destroying all internal structures in the affected intervals.

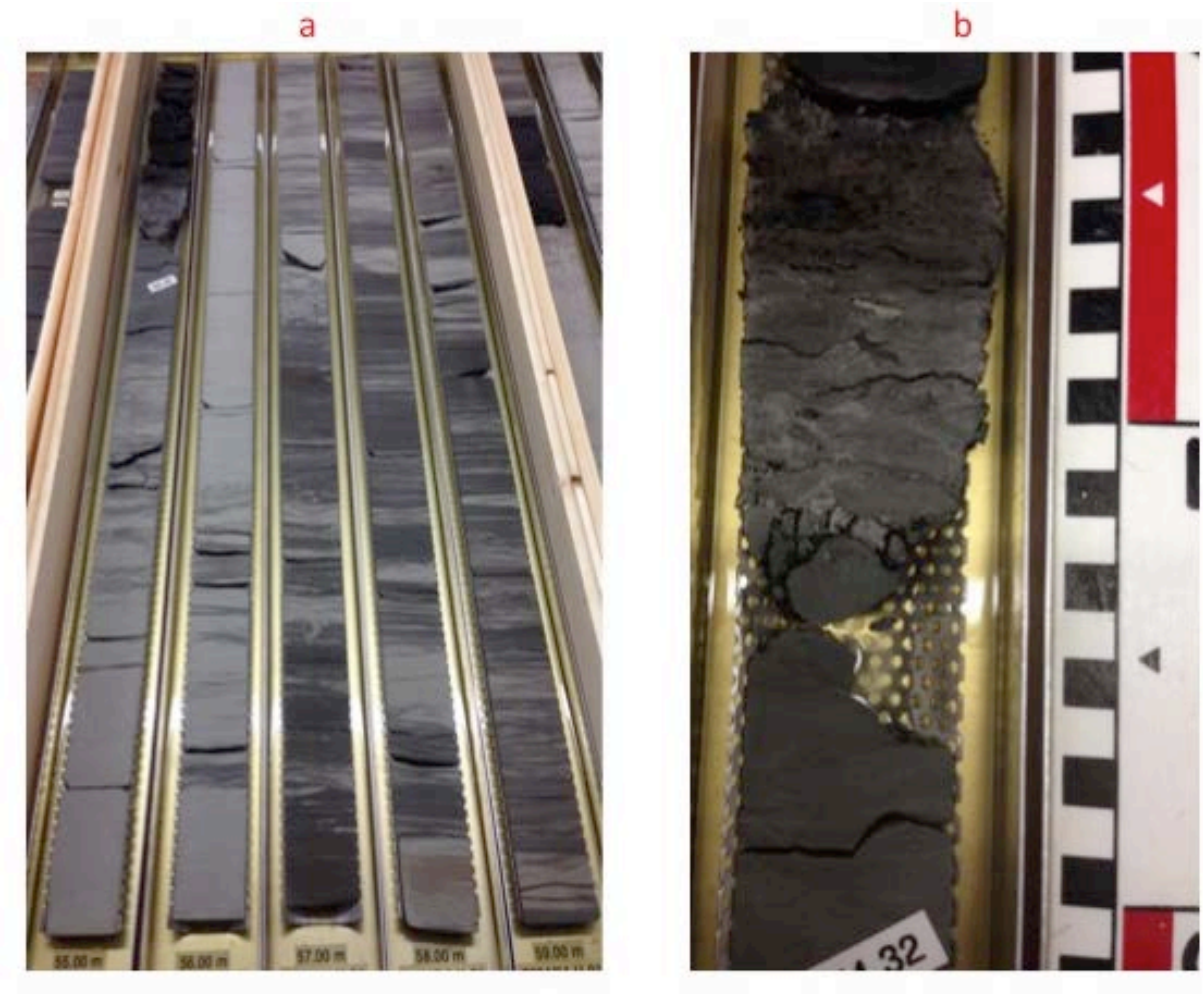

Figure 4.5: Main lithologies of unit D. Coarsening upwards parasequence capped with coal (a). Paleosol with roots (b).

4.3 Palynofacies Analysis

The quantitative results are displayed in figure 4.6, and are also included in the combined range chart together with the recordings from the quantitative palynology (Appendix II). The recorded abundances have also been plotted in two separate ternary plots (fig. 4.8 and 4.9). According to Tyson (1995), these plots provide important information that may be useful for palaeoenvironmental interpretation. The combining of these plots together with sedimentological evidence and palynofacies estimates will be discussed in chapter 5.2.

The lowermost interval show highly fluctuating trends in the palynofacies. It comprises the seven lowermost samples, taken from 233.48 m to 200.74 m (fig. 4.6). The interval is initiated at 233.48 m with a total dominance of amorphous organic matter (AOM) (fig. 4.7a), accounting for almost 100% of the palynofacies. Similar relative abundances is recorded in the overlying sample at 226.72 m, however with slightly increased amounts of phytoclasts. The remaining five samples fluctuate between dominance of AOM (> 90%) to total absence of AOM, in which the abundances are affiliated relatively even distribution of phytoclasts (mainly gelified woody tissue and wood tracheids (fig. 4.7d,e) and sporomorphs. The general trend shows an overall upward increase in terrestrially derived organic matter. Low amounts of plant cuticles (1-3%)(fig. 4.7c) were recorded in the phytoclast-dominated samples.

The next interval, corresponding to the samples at 197.38-153.55 m, display very similar trends as described from in the underlying 33 meters (fig. 4.6). A reinitiation of AOM dominant abundances is recorded in the three lowermost samples (197.38 m, 194.53 m and 189.66 m). Fluctuations between AOM abundant and phytoclasts-sporomorph abundant samples characterize the remaining nine samples of this interval. Five of these nine last samples are dominated by AOM (179.33 m, 175.10 m, 171.83 m, 163.48 m and 154.17 m). However, an upward decline in this dominance is recorded, going from 74 % AOM in the sample from 179.33 m to 54 % in the sample from 154.17 m. An overall upward increase of terrestrially derived organic matter is also recorded, in similar ways as observed in the underlying interval. Small amounts of plant cuticles (2-3 %) were also recorded in the samples from 175.10 m, 169.00 m and 159.90 m.

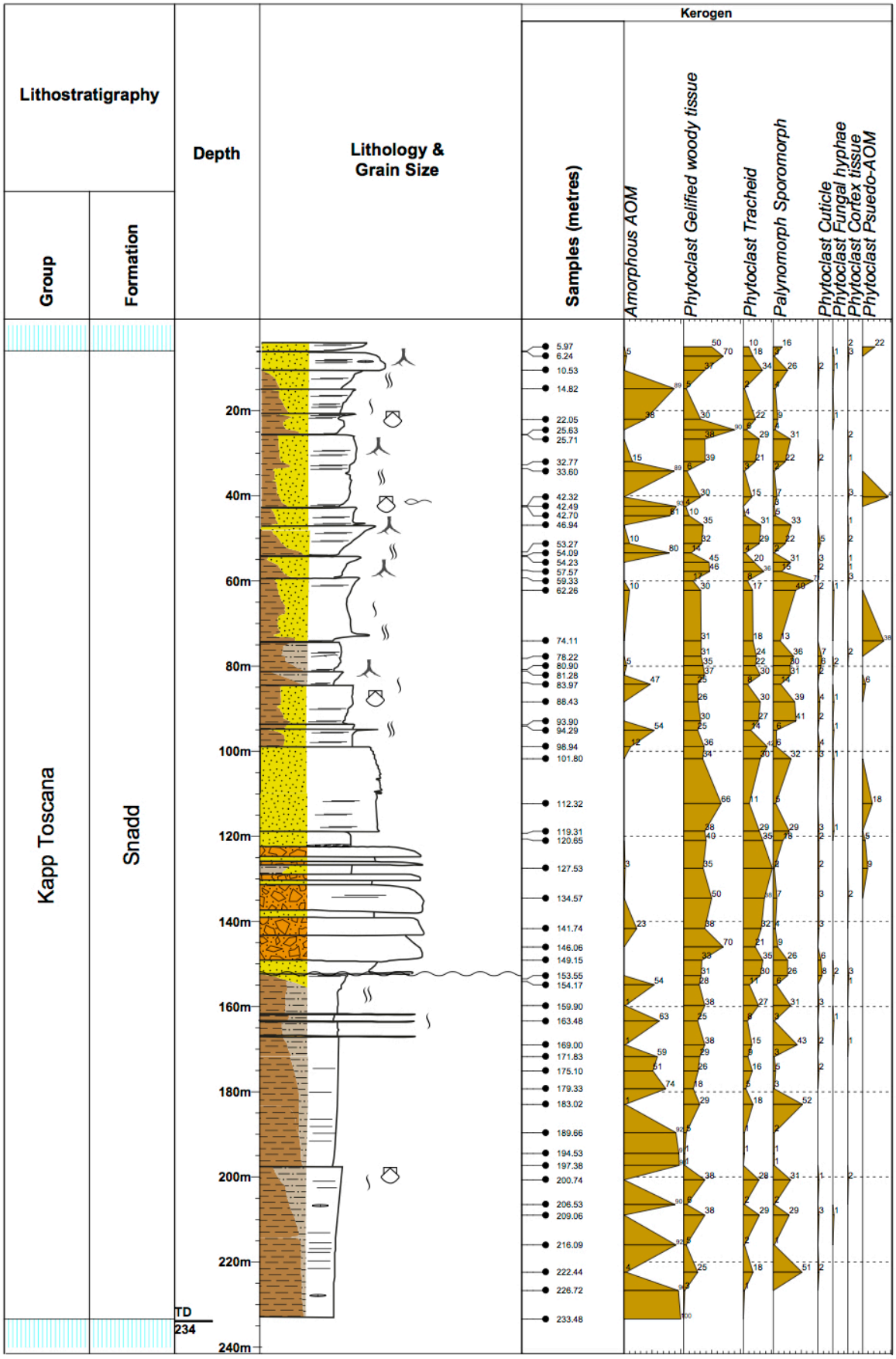

Figure 4.6: Abundance of particulate organic matter (POM) and cropped log of core 7534/4-U-1 with corresponding locations of the analyzed samples.

An additional remark regarding the two lowermost intervals: the fluctuations seen in the two lowermost intervals seem to be related to the two different sample sets. The newer samples constitute the estimates that lack the dominant abundance of AOM. If this should prove to be caused by different preparation methods between the different laboratories, the results of these samples should be regarded as uncertain. However, it is still possible that this trend reflect palaeoenvironmental events (further discussed in chapter 5.2).

A marked change is recorded in the overlying interval between 149.15-101.80 m. The interval represents nine samples predominantly abundant in phytoclasts. Gelified woody tissue and wood tracheids constitute the main components in all these samples. One exception is the sample from 141.74 m, which held a significant amount of AOM (23%), however not dominant. An additional remark on this interval is the first consistent presence of large plant cuticles, along with lesser portions of cortex tissue (fig. 4.7b) and fungal hyphae. Sporomorphs also has a substantial presence within this interval, especially within the samples at 149.15 m, 120.65 m, 119.31 m and 101.80 m.

The uppermost interval comprises the remaining 28 samples. A fluctuating trend characterizes this interval, and does remind of the two lowermost intervals. However, an overall dominance of phytoclasts is recorded (as opposed to the AOM dominated lower intervals). A dominance of sporomorphs is recorded in the sample from 59.33 m. Occasional dominance of AOM. Plant cuticle, fungal hyphae and cortex tissues were all recorded in lesser amounts with sporadic occurrence. The main constituents in the phytoclast dominated samples comprise gelified woody tissues and wood tracheids. The lower samples dominated by AOM (94.29 m and 83.97 m) still contains substantial amounts of phytoclasts, with the estimated abundance affiliated to AOM varying between 47-54 %. However, the upper AOM dominated samples (54.09 m, 42.70 m, 42.49 m, 33.60 m and 14.82 m) are swamped with the amorphous material, accounting for 80-93 % of the total abundance.

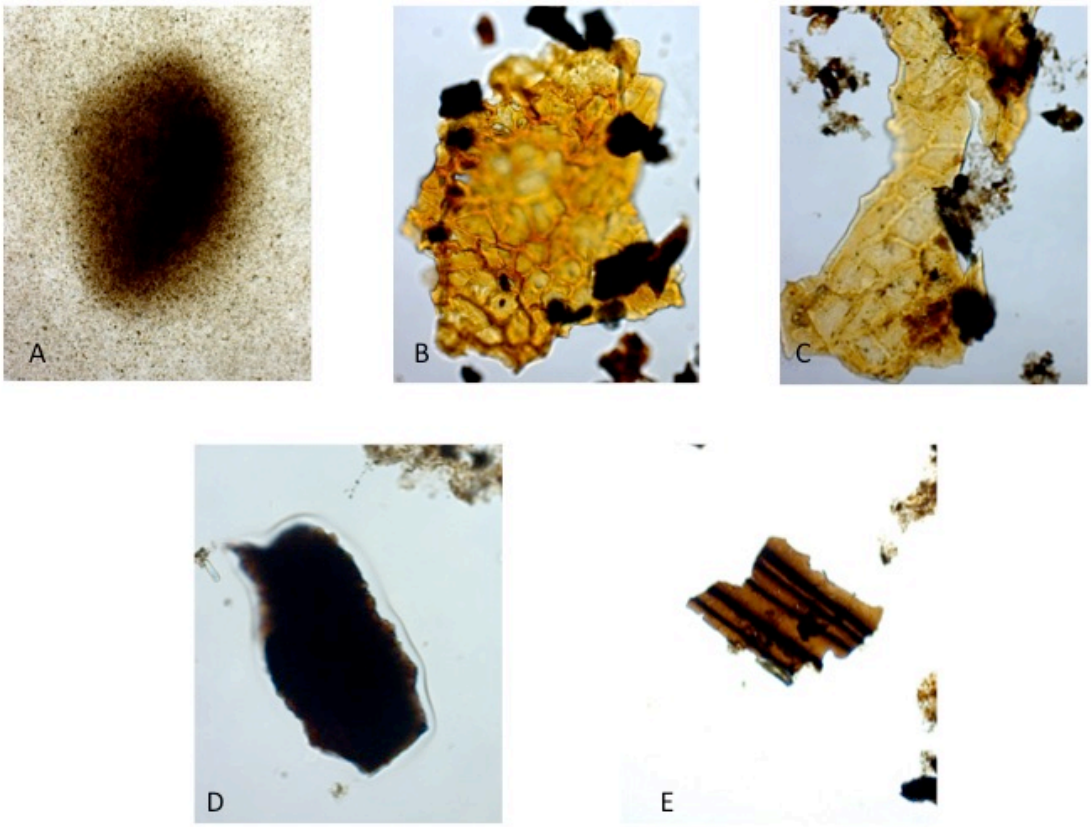

Figure 4.7: Main constituents recorded in the palynofacies analysis; (A) amorphous organic matter (AOM), (B) cortex tissue, (C) plant cuticle, (D) gelified woody tissue, (E) wood tracheid. Sporomorphs are not included (see appendix V).

Ternary plots

The AOM-Palynomorph-Phytoclasts (APP) plot was conducted in order to characterize the paleoenvironment and thereby provide information on the differences in relative proximity to terrestrial organic matter sources represented by the samples and associated "kerogen transport paths", as explained by Tyson (1995). High dominance of AOM is typically related to suboxic-anoxic marine environments, where it often occurs in great enough amounts to "overprint" the terrestrial material given that these reducing conditions are present (Tyson, 1995). A large amount of the samples show relatively high palynomorph percentages (>10%) and high phytoclasts percentages (>50%) and are apparently characteristic only of some shallow shelf settings (Tyson, 1995) (fig. 4.8). According to Tyson (1995), the information

provided from this plot can be joined with the previously explained observations (palynofacies estimates) to emphasize on the paleoenvironmental interpretation.

The plot of these individual kerogen samples reveals mainly two “kerogen transport paths”. The dominant part of the samples plot within zone “I” and “III”, assigned to “highly proximal shelf or basin” and “heterolithic oxic shelf (proximal)” (fig. 9). These samples were mainly related to the spore dominated assemblages recorded in the upper part of the core.
Further on, a large portion of the samples plot within zone “IX” corresponding to a “distal suboxic-anoxic basin” (fig. 9), resembled by the lowest part of the core dominantly composed of mudstone.

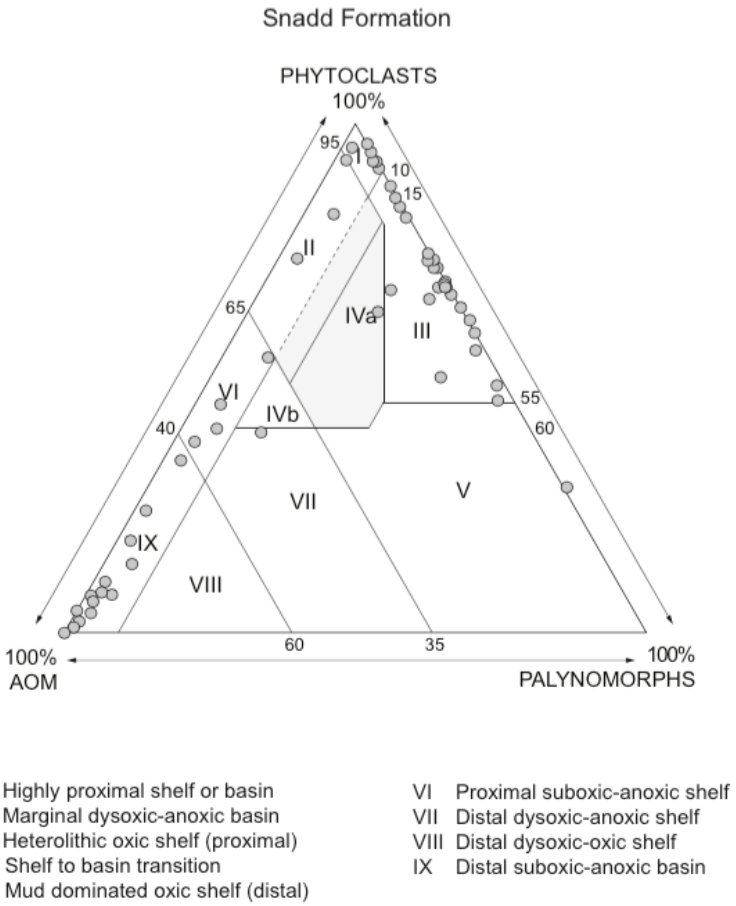

Figure 4.8: AOM-Palynomorph-Phytoclasts (APP) ternary plot of kerogen samples from core 7534/4-U-1 (after Tyson 1985, 1989, 1993).

The Spore-Pollen-Microplankton (SPM) plot includes valuable information of how the changing abundances in quantitative palynology relates to depositional environment. This plot was only based on the counted samples, and display a distinct separation between the upper and lower part of the core. One can observe a clear distinction between the lowermost interval between 233.48 – 153.55 m and the upper interval between 98.94 – 6.24 m. The plot indicates an offshore – nearshore marine environment for the lower shale unit, and a fluvio-deltaic signature for the upper unit. This will be combined in the discussion, together with the evidence obtained from the core description and palynofacies analysis.

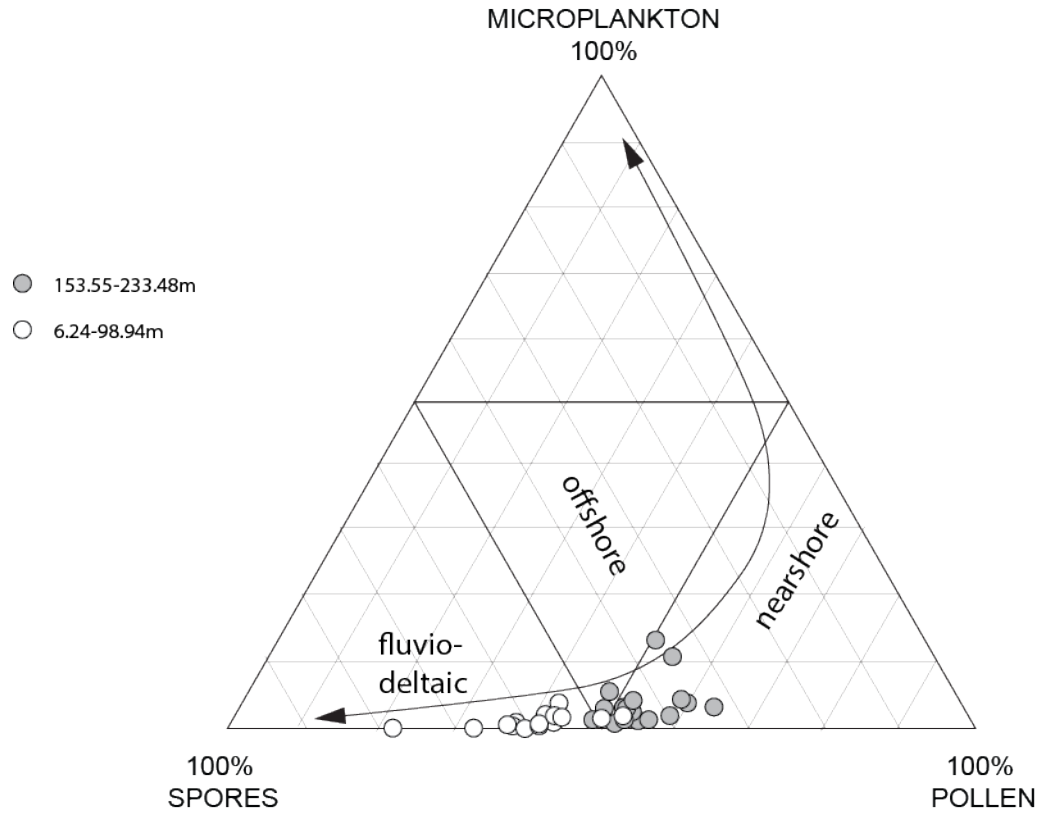

Figure 4.9: Spore-Pollen-Microplankton (SPM) ternary plot for core 7534/4-U-1 (after Federova, 1977; Traverse, 1988; Duringer and Doubinger, 1985).

5. Discussion

5.1 Palynostratigraphy

Core 7534/4-U-1 has previously been suggested to be of early Carnian age (Julian) by Vigran et al. (2014), and they assigned the assemblage to their *Aulisporites astigmosus* Composite Assemblage Zone (fig. 5.2). No quantitative data was however, provided. The most significant features throughout the assemblages have been described in chapter 4.1.

The present study has revealed three distinct palynological assemblages (see chapter 4.1) within this core ranging from the lowermost assemblage dominated by bisaccate pollen including rich amounts of the *Triadispora* genus, up through an assemblage with a marked increase *Krauselisporites* spp., *Krauselisporites cooksonae* and *Aratrisporites* spp. and followed by the youngest assemblage characterized by an acme of the monolete spore *Leschikisporis aduncus.*

These individual assemblages will be discussed in order to further constrain the age of core 7534/4-U-1.

Assemblage SB-I

This oldest assemblage from core 7534/4-U-1 is dominated by bisaccate pollen, comprising the highest abundances of *Triadispora* spp., *Lunatisporites* spp. and *Striatoabieites balmei* throughout the succession, and with consistent but rare occurrence of *Angustisulcites klausii* (Appendix II). It correlates well with Floral Phase 10 of Hochuli and Vigran (2010)(fig. 5.1), which is dominantly composed of non-taeniate bisaccate pollen. They reported reduced occurrence of taeniate bisaccate pollen compared to their underlying phase 9 (Hochuli and Vigran, 2010). Taeniate bisaccate pollen is consistently present in Assemblage SB-I (Appendix II), however, in low numbers. It is worth mentioning that various long-ranging marine acritarchs has the highest abundance in this assemblage, with the majority affiliated to *Michrystridium* spp.

Floral Phase 10 of Hochuli and Vigran (2010) was marked by a decrease in the conifer pollen groups *Ovalipollis*/*Illinites* (compared to phase 9). The quantitative data recorded herein fit well with their abundance data for these groups. A slightly diminishing trend of the coastal conifer pollen *Araucariacites australis* has been recorded in Assemblage SB-I, which further supports the assemblage to predate the overlying phase 11 of Hochuli and Vigran (2010).

Hochuli and Vigran (2010) correlated their floral phases to the previous palynozonations established by Hochuli et al. (1989). Floral phase 10 was suggested to correlate with Assemblage H-G with the upper part possibly reaching into Assemblage F. This correlation places the recorded assemblages into the mid-Upper Ladinian, with a possibly earliest Carnian age in the upper part. The characteristics of Assemblage G and H of Hochuli et al. (1989) fit well within the recorded taxa of Assemblage SB-I.

It is worth noting that none of the characteristic taxa with last appearance in the underlying Assemblage I of Hochuli et al. (1989) has been recorded in core 7534/4-U-1. The taxa include *Bhardawajispora labichensis*, *Cordaitina gunyalensis, Dyupetalum* cf. *vicentinensis* and *Judasporites* spp.. However, all their taxa, with one exception (*Diplicisporites granulatus*), listed to range up from Assemblage I into H-G (of Hochuli et al., 1989), are also recorded herein. This includes *Echinitosporites iliacoides, Krauselisporites cooksonae, Ovalipollis*

pseudoalatus, Schizaeoisporites worsleyi, Thomsonisporites toralis and *Triadispora verrucata*. Assemblage I of Hochuli et al. (1989) has been calibrated to the *Indigrites varius* Ammonite Zone found in the Bravaisberget Formation at Festningen, and within other wells in the Barents Sea, corresponding to an early Ladinian age (Hochuli et al., 1989).

The tentative correlations and negative evidence discussed above suggests a younger age than early Ladinian for Assemblage SB-I of core 7534/4-U-1. The correlation to similar assemblages with independent dating (obtained from ammonite zones) provide for a more reliable age assignment. The total absence of the gymnosperm pollen *Aulisporites astigmosus* also support that this assemblage predates the early Carnian stage, where this species is regarded to have its FO (first occurrence)(Vigran et al., 2014).

The sedimentological description of core 7534/4-U-1 show an erosional contact corresponding to the top of Assemblage SB-I, possibly representing a hiatus between Assemblage SB-I and the overlying Assemblage SB-II (see fig. 4.1 and Appendix II).

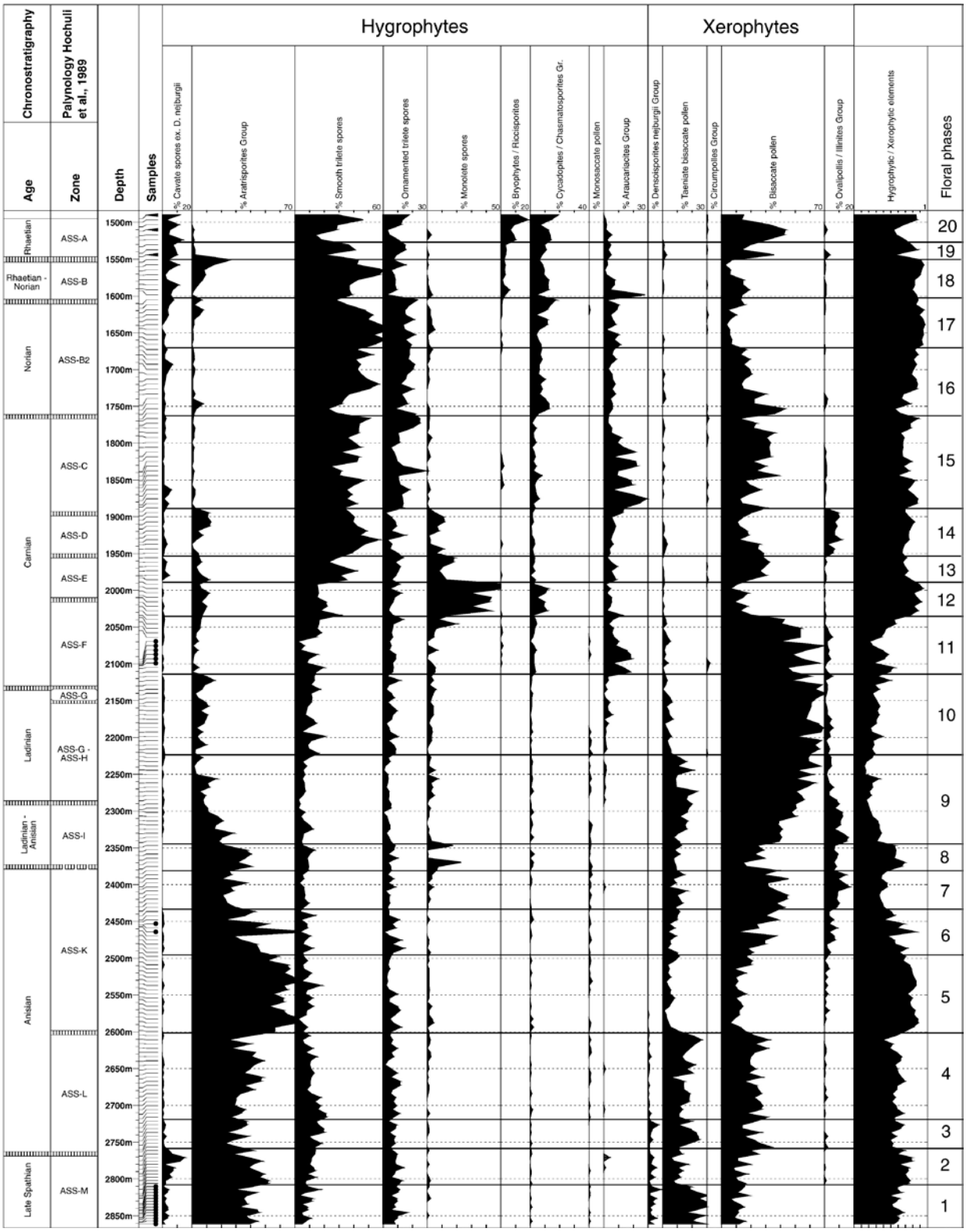

Figure 5.1: Floral phases (1-20) established by Hochuli and Vigran (2010) based on relative abundances recorded through a well from the Nordkapp Basin. The floral phases is correlated with the established palynozonations of Hochuli et al. (1989) (from Hochuli and Vigran, 2010).

Assemblage SB-II

A significant characteristic and marker for Assemblage SB-II is an acme of the cavate, trilete spore *Krauselisporites* spp., recorded at 83.97 m, in addition to common occurrence of *Krauselisporites cooksonae*. Additionally, an increase in the lycopsid spore genera *Aratrisporites* were recorded within this spore dominated assemblage. The abundance of bisaccate pollen decrease significantly compared to the underlying Assemblage SB-I, as previously explained in chapter 4.1. Vigran et al. (2014) also recorded common presence of *Krauselisporites* spp. within this interval of core 7534/4-U-1, especially in the sample at 83.97 m.

Assemblage SB-II seems to potentially correlate with Assemblage F of Hochuli et al. (1989), although several differences including the quantitative occurrence of taxa like *Striatoabieites* spp. and *Lunatisporites* spp. are different. Presence of *Angustisulcites klausii* and *Podosporites amicus* in Assemblage SB-II is consistent with the occurrences in Assemblage F of Hochuli et al. (1989). Important to note is the first occurrence of the conifer pollen *Aulisporites astigmosus*. This species was also reported to have its earliest occurrence in their Assemblage F, and the species was also used to define the *Aulisporites astigmosus* Composite Assemblage Zone of Vigran et al. (2014), marking the base Carnian. An early Carnian age was assigned to Assemblage F based on calibration to ammonites collected from the Tschermakfjellet Formation, and placed within the *Stolleites tenuis* Zone (Hochuli et al., 1989).

The occurrence of *A. astigmosus* is also regarded as a marker for the early Carnian (Julian) in the Alpine realms (Cirilli, 2010). However, as previously mentioned, several authors (Hochuli et al., 1989; Hochuli and Vigran, 2010) record significant differences between the assemblages from the Boreal and Alpine realm. The paleolatitudinal (and climatic) differences between these two regions is a likely cause for this (Paterson et al., submitted).

Assemblage F of Hochuli et al. (1989) was included in Floral Phase 11 of Hochuli and Vigran (2010)(fig. 5.1). The upper part of this phase is characterized by an increase in monolete and trilete spores (Hochuli and Vigran, 2010)(fig. 5.1). Further on, the floral phase was defined by

a peak in the *Araucariacites* genus, and a rare but continuous presence of *Chasmatosporites* spp. (Hochuli and Vigran, 2010). This fits the observations recorded in Assemblage SB-II. Taeniate bisaccates (e.g. *Lunatisporites* and *Striatoabieites*) were proposed to have a fading occurrence in this phase, as opposed to a common presence in older assemblages. The sporadic and rare occurrence of these genera within Assemblage SB-II further supports a correlation to Floral Phase 11 of Hochuli and Vigran (2010).

The underlying Floral Phase 10 of Hochuli and Vigran (2010) is defined by a common occurrence of non-taeniate bisaccates, and a rare but consistent occurrence of the *Araucariacites* group. The latter group has been recorded in very common amounts, which contradicts a placement of Assemblage SB-II within Floral Phase 10.

A similar assemblage has been recorded by Paterson et al. (submitted) from core material located offshore Kong Karls Land. The most pronounced feature of their assemblage is the acme of the lycopsid spore *Krauselisporites* spp.. The abundant spore and pollen taxa recorded by Paterson et al. (submitted) show high similarity to the recordings herein. Marine palynomorphs were also present in the Kong Karls Land assemblage, in an equally rare manner as observed in this study. The acritarchs *Michrystridium* spp. and *Veryhachium* spp. were the recorded taxa. The freshwater palynomorph *Botryococcus* spp. was recorded in sample 62.26 m.

A significant difference in the abundance of the long-ranging taxa of Assemblage SB-II differentiates it from the '*Leschikisporis aduncus* assemblage' of Paterson and Mangerud (2015). These abundances may very well represent an environmental signature, at least for the acmes, which only are recorded in a few samples. However, it is still likely that these trends represent palynofloral events of biostratigraphic importance in correlation. The monolete fern spore *Leschikisporis aduncus* has been recorded in common amounts in Assemblage SB-II, but does not reach the same abundances as documented for the late Carnian '*Leschikisporis aduncus* assemblage' of Paterson and Mangerud (2015). Assemblage SB-II is thus tentatively assigned to an early Carnian (Julian) age.

The taxon *Echinitosporites iliacoides*, previously considered as a confident marker for a Ladinian age, is regarded to have its FAD in Assemblage G of Hochuli et al. (1989).

Assemblage G was recorded from the Skuld Formation on Bjørnøya by Mørk et al. (1990) (among other localities). The presence of the ammonite *Daxatina canadensis* within these deposits was recorded and co-occurred with *E. iliacoides*. Due to recent revision of the geological timescale by Ogg et al. (2008), the *D. canadensis* Zone is now regarded to represent the base Carnian, effectively pushing the range of *E. iliacoides* up into the Carnian (Vigran et al., 2014).

Assemblage SB-III

The *Leschikisporis aduncus* acme is the most prominent feature of Assemblage SB-III. This acme has been recorded in several previous studies from the Barents Sea area, including Paterson and Mangerud (2015), Holen (2014), Ask (2013), Hochuli et al. (1989), Hochuli and Vigran (2010), Bjærke and Manum (1977), Nagy et al. (2011) and Vigran et al. (2014). All these records are assigned a mid-late Carnian age, and recently to the Tuvalian (2-3) by Paterson and Mangerud (2015).

The Floral Phase 12 of Hochuli and Vigran (2010) is characterized by a *Leschikisporis aduncus* acme, which seems to occur in one single event with no further peaks in abundance neither above nor beneath this phase (fig. 5.1). The transition into phase 12 is marked with a significant floral change; going from conifer dominated assemblages of phase 11 to fern dominated assemblages of phase 12 (Hochuli and Vigran, 2010). Common occurrences of smooth trilete spores and sporadic occurrence of taeniate bisaccates also characterize Floral Phase 12, which is consistent with the recordings in Assemblage SB-III.

The occurrences described in assemblage D and E of Hochuli et al. (1989) correlate well with the recordings in Assemblage SB-III. Assemblage E was also partly included in Floral Phase 12 of Hochuli and Vigran (2010). Assemblage D of Hochuli et al. (1989) is defined by common occurrences of conifer pollen, mostly affiliated to the *Triadispora*, *Brachysaccus* and *Ovalipollis* genera. *Triadispora* and *Ovalipollis* have been recorded in this assemblage, though not present in very common amounts. The common spore taxa of Assemblage D include *Leschikisporis aduncus*, *Punctatisporites walkomii* and *Gibeosporites lativerrucosus*

(Hochuli et al., 1989). The first downhole appearance of the following taxa indicates the top of Assemblage D; *Aulisporites astigmosus*, *Camerosporites secatus*, *Duplicisporites granulatus*, *Illinites chitinoides*, *Infernopollenites sulcatus*, *Krauselisporites cooksonae*, *Kuglerina meieri*, *Triadispora plicata* and *Uvaesporites gadensis* (Hochuli et al., 1989). *Aulisporites astigmosus*, *Illinites chitinoides* and *Krauselisporites cooksonae* were also recorded in this study. Assemblage E has very similar characteristics but is, according to Hochuli et al. (1989), distinguished from Assemblage D by an abundance decrease in *Ovalipollis*, and still a dominating occurrence of *Leschikisporis aduncus* and *Triadispora*. Dominance of *Triadispora* was not recorded in assemblage SB-III.

Assemblage SB-III show high similarity to the late Carnian '*Leschikisporis aduncus* assemblage' of Paterson and Mangerud (2015)(fig. 5.2). They proposed the assemblage to correlate to Assemblage D and E of Hochuli et al. (1989), as also suggested for Assemblage SB-III herein. Dominance of *Leschikisporis aduncus* was also reported by Vigran et al. (2014) in their *A.* astigmosus Composite Assemblage Zone. The rare and sporadic presence of *Echinitosporites iliacoides* in this uppermost assemblage has also been recorded by Vigran et al. (2014), and may indicate an extended range of this species compared to previous studies. Alternatively it could represent reworking. However, based on the consistent occurrence and similar preservation of this taxon throughout core 7534/4-U-1, reworking is dismissed.

The late Carnian Assemblage C of Hochuli et al. (1989) is characterized by a dominance of conifer pollen grains, with high abundance of the *Protodiploxypinus* genus. This trend has also been recorded in the late Carnian Floral Phase 15 of Hochuli and Vigran (2010)(fig. 5.1), and the *Protodiploxypinus* spp. assemblage of Paterson and Mangerud (2015)(fig. 5.2). A high abundance of this genus has not been recorded in this Assemblage SB-III.

Assemblage C of Hochuli et al. (1989) is also characterized by the oldest occurrences of dinoflagellate cysts, which later become common in the Norian Assemblage B-2 (Hochuli et al., 1989). It is therefore important to note that no dinoflagellate cysts were recorded in core 7534/4-U-1.

Based on these observations, Assemblage SB-III most likely predates the Norian influx of dinoflagellates, and the dominance of conifer pollen previously recorded in latest Carnian assemblages (Hochuli et al., 1989; Hochuli and Vigran, 2010; Paterson and Mangerud, 2015)(fig. 5.2). The most likely age of Assemblage SB-III is mid-late Carnian. Assemblage SB-III is closely comparable to assemblage D and E of Hochuli et al. (1989), Floral Phase 12 of Hochuli and Vigran (2010), the lower part of *Aulisporites astigmosus* Zone of Vigran et al. (2014) and the *Leschikisporis aduncus* assemblage of Paterson and Mangerud (2015). The *L. aduncus* acme is likely to have a palaeoenvironmental relation, with deposits located very proximal to fern inhabited swamps, but is still believed to represent a significant biostratigraphic marker of vast regional importance resulting from a widespread floral event.

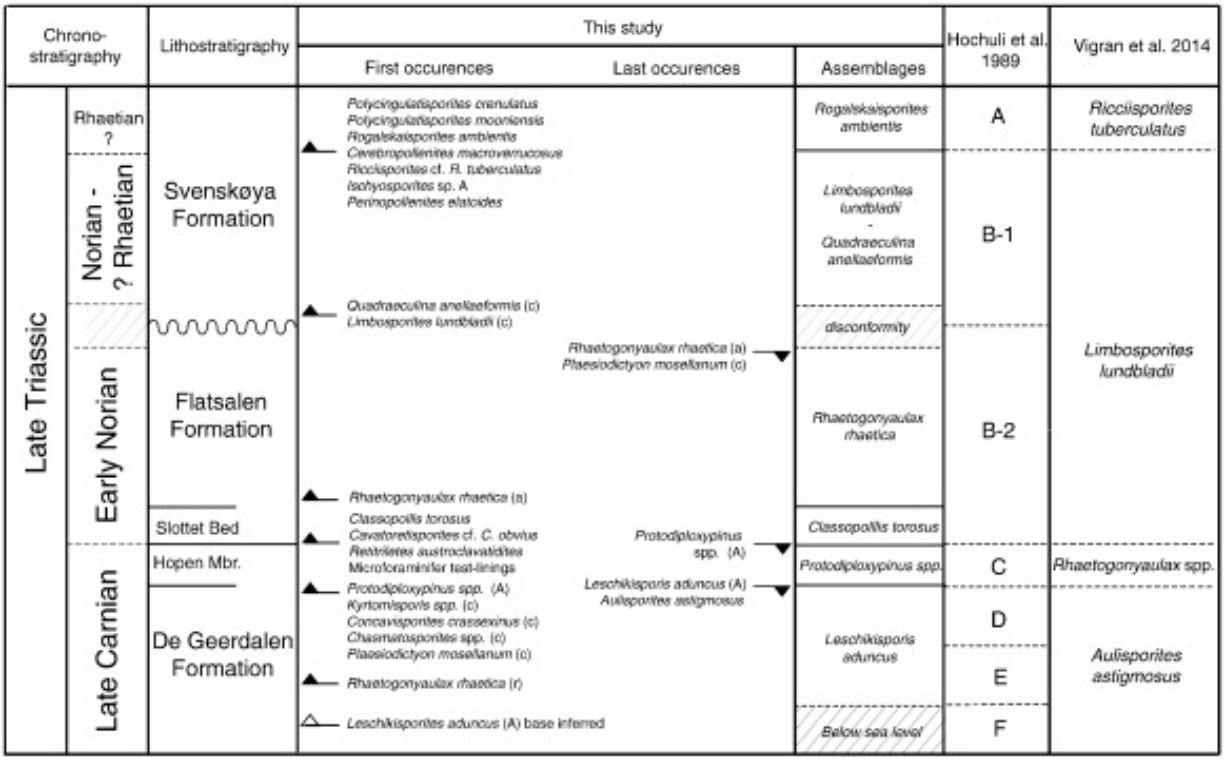

Figure 5.2: Proposed palynological succession of Paterson and Mangerud (2015) for their Hopen assemblages. The relation to the previously established zonations of Hochuli et al. (1989) and Vigran et al. (2014) are illustrated. (A) = acme, (a) = abundant, (c) = common, (r) = rare (from Paterson and Mangerud, 2015).

Summary

The most likely age for core 7534/4-U-1 is late Ladinian to mid-late Carnian (Tuvalian). This conclusion has been reached based on the correlations to previous zonations, along with negative evidence in order to constrain the timeframe of the deposits. The correlation of each assemblage has been bounded by independent datings from ammonite zones, providing for a more reliable age determination. Presence of *Aulisporites astigmosus* (upper two assemblages) and *Echinitosporites iliacoides* most likely indicates an overlap between the Ladinian *Echinitosporites iliacoides* Zone and the early-mid Carnian *Aulisporites astigmosus* Zone of Vigran et al. (2014). Negative evidence has also been applied to strengthen the age interpretation; absence of dinoflagellate cysts suggests the succession to predate the latest Carnian to Norian age based on correlation to Hochuli et al. (1989), Vigran et al. (2014), Paterson and Mangerud (2015), Vigran et al (1998) and Hochuli and Vigran (2010). The lowermost part of the core most likely represents younger deposits than early Ladinian, with evidence suggesting it to postdate the Assemblage I of Hochuli et al. (1989), Svalis-8 of Vigran et al. (1998) and Floral Phase 9 of Hochuli and Vigran (2010). The tentative correlation between core 7534/4-U-1 and the discussed works are presented in figure 5.3.

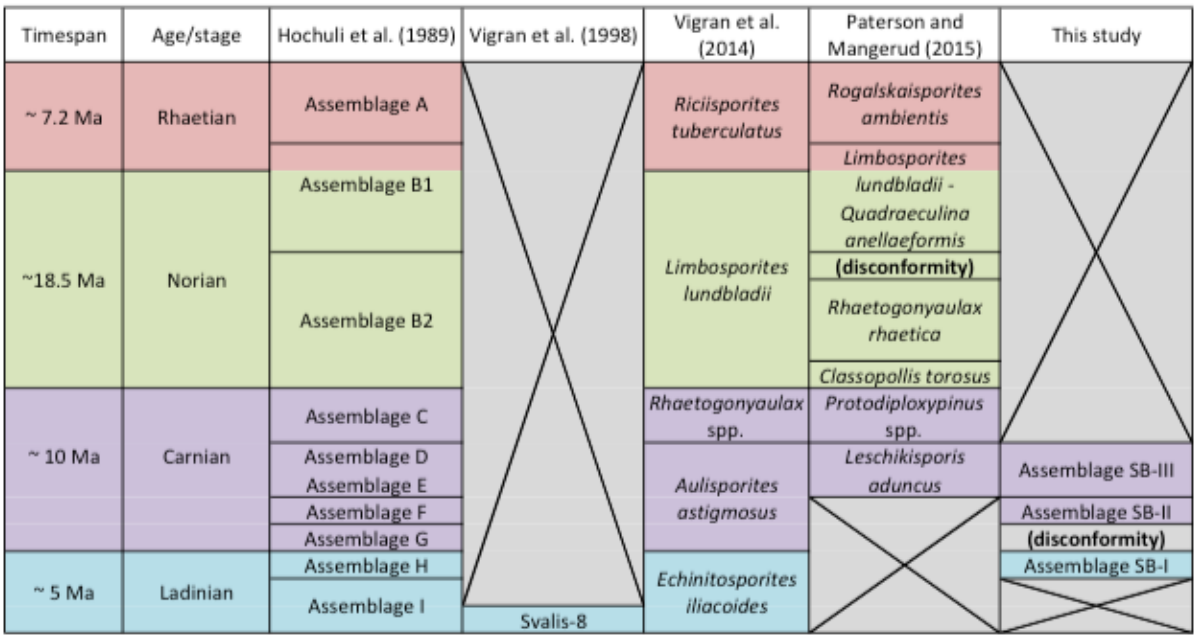

Figure 5.3: Proposed correlation between core 7534/4-U-1 and previously established zonations. Timespan estimated based on approximates from the ICS-chart v2015. See fig. 12 for relation between floral phases of Vigran and Hochuli (2010) and established assemblages from Hochuli et al. (1989).

5.2 Paleoenvironment

The four sedimentological units described in chapter 4.3 is discussed below in a depositional environmental context and tried linked to palynofacies as well as the quantitative palynological analysis.

Unit A (233.48 m – 152.80 m)

This unit comprises a fairly uniform interval of shale with two coarsening upwards sequences (233.50-198.10 m and 198.10-152.80 m) grading from dark organic-rich mudstone into muddy grey siltstone (fig. 4.1). The unit is interpreted as a prodelta deposit, which typically produces coarsening-upward sequences with increasing proximity to the delta-front, and is commonly composed of muddy facies (Elliot, 1986; Coleman and Wright, 1975). Thicknesses of these successions may vary from meters to hundreds of meters, depending on the scale of the delta, water depth and subsidence rate (Bhattacharya, 2006). The thickness of unit A, of approximately 80 m, indicates a prevalent deltaic system. Evidence of minor bioturbation in finely laminated, organic rich shales suggests a marine environment. This is confirmed by the common occurrence of marine acritarchs (mainly *Michrystridium* spp.). The peak abundances of these acritarchs coincide with the bottommost part of both these coarsening upwards sequences. The upper section of the core contains three thinbeds of pebble conglomerate, interpreted to be storm deposits, placing this upper part above the storm-weather wave-base. Additionally, ripple lamination were observed in the very top of both the sequences, placing these parts above fair-weather wave-base.

The palynofacies analysis revealed the dominance of amorphous organic matter (AOM), variably degraded phytoclasts (tracheid/gelified woody tissue/cuticles) and palynomorphs. Particulate organic matter (POM) assemblages from the lowermost part displayed a composition dominated by AOM followed by an upward increase of wood fragments up to and including sample 200.74 m (fig. 5.4). Minor presence of large cuticle fragments suggests deposition to be within the reach of a terrestrial source, in a marginal setting. Above the boundary at 198.10 m there was observed an influx of AOM abundant composition, which

corresponds well with the deposition of similar organic-rich shales as seen in the lowermost part (fig. 5.4). The same trend is observed in this uppermost sequence, with an upward increase in phytoclasts up to and including sample 153.55 m. These upward changing trends coincide with the two upward coarsening sequences of shale, and indicates increasing proximity to terrestrial kerogen sources and transition into an oxic environment, causing terrestrial derived organic matter to gradually overprint the AOM abundance. The samples dominated by AOM suggest deposition under dysoxic-anoxic conditions, in addition to a low input of terrestrial material (Tyson, 1995). This could be caused by changing delta lobes (Riis et al., 2008) or progradation of the delta-front. The interval has consequently been interpreted as a marine environment, in a prodelta setting.

The evidence from the APP ternary plot is also consistent with this interpretation (fig. 4.8). The samples corresponding to this unit fluctuates between “distal suboxic-anoxic basin” and “Heterolithic oxic shelf (proximal)”, which reflects the changing abundance between AOM dominance and phytoclast dominance within these deposits. A nearshore-offshore environment is also supported by the SPM ternary plot (fig. 4.9).

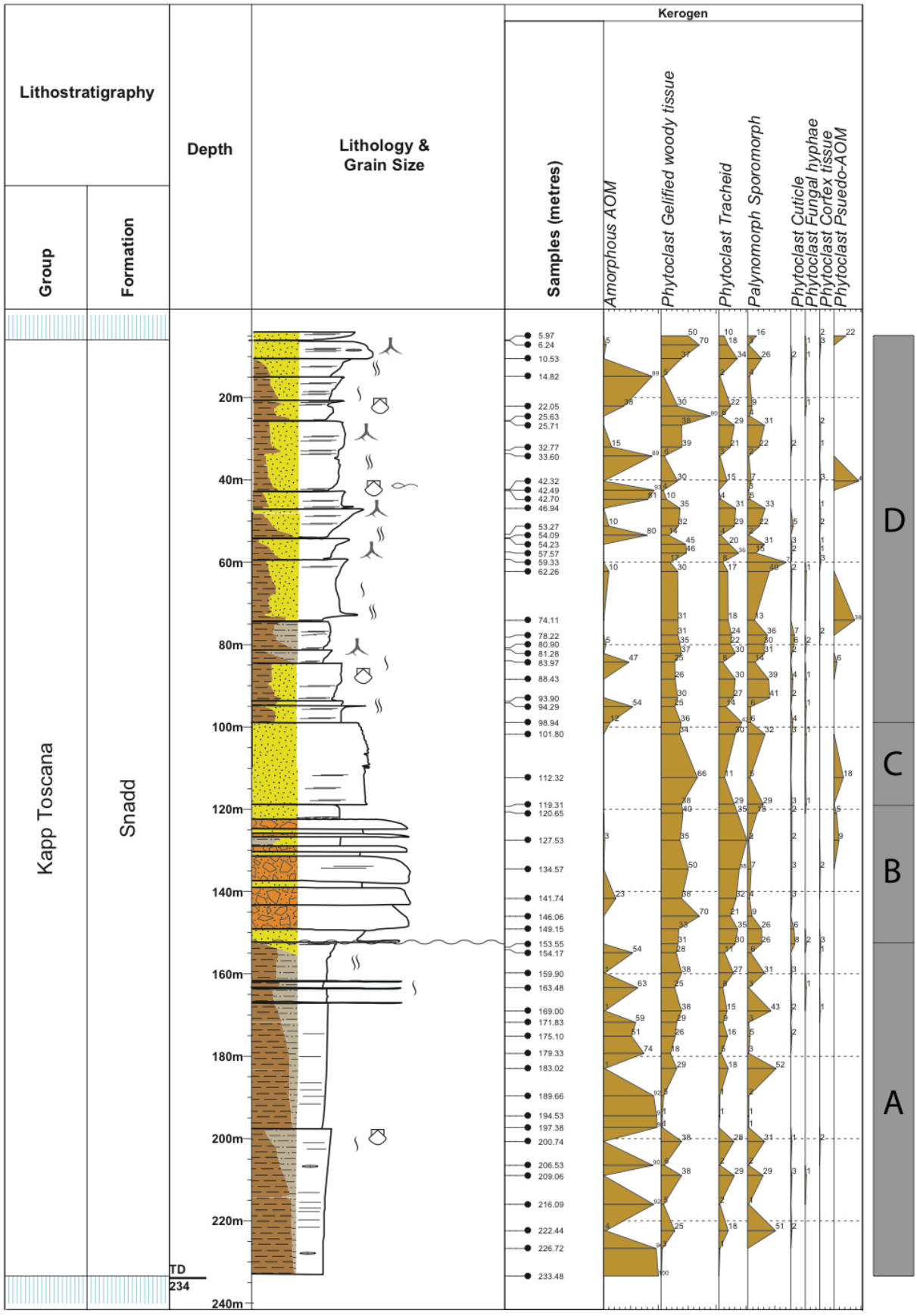

Figure 5.4: Relative POM abundances recorded in the palynofacies analysis put in relation to the divided facies associations (far right) and the cropped log of core 7534/4-U-1. Note the unconformable contact at 152.80m.

Unit B (152.80 m – 119.05 m)

An erosional boundary at 152.80 m initiates this unit, representing a significant change in lithology from the underlying shales. Intraformational conglomerate beds with fining upward trends punctuated by finer sandstone and mudstone beds characterize this interval (fig. 4.1). This unit has been interpreted to represent channel system deposits. The angular texture of the rip-up clasts in the conglomerate indicates a very short transport distance and rapid deposition. The mud deposits have not been fully lithified as soft sediment deformation is observed within these clasts (visible in fig. 4.3a). Two beds of interlaminated sand and silt was observed in the upper part of this unit, and has been interpreted to be overbank deposits. The rhythmical deposition of sand-mud reflects pulses of sediment input from the distributary channel, followed by calm conditions which allow fine sediment to settle out of suspension.

This interval has previously been interpreted to represent a tide-influenced delta front (Riis et al., 2008; Høy and Lundschien, 2011; Lundschien et al., 2014). The observations of the particulate organic matter in this study reveal a total dominance of phytoclasts, indicative of a terrestrial environment (fig. 5.4). A higher consistency and abundance of leaf cuticles, coupled with presence of coal debris in these deposits indicates an environment highly proximal to terrestrial kerogen sources. It is likely that the rapid deposition of the sequence led to an unfavorable environment for living organisms, a point made by Riis et al. (2008), as no signs of bioturbation are present within this unit. In a tidal environment one would still expect some marine components in the quantitative palynology. However, no marine records are detected in the present study. This latter evidence combined with a total dominance of terrestrially derived material within the deposits, suggests the succession to represent a terrestrial channel system, with minimal to no tidal influence.

This facies change may be regional. The erosional boundary at 152.80 m corresponds to a regional seismic sequence boundary, as documented by Riis et al. (2008). This boundary separates open marine and delta plain seismic facies, indicating that a regional sea-level fall has led to forced channel incision and deposition of these intraformational conglomerates, as observed in core 7534/4-U-1 (Riis et al., 2008). The results obtained from this study are

consistent with this interpretation. Highly different composition in palynofacies between Unit A and B is suggestive of a major shift in depositional environment (fig. 5.4). The dominance of phytoclasts within these deposits is represented in the APP ternary plot, of which the majority of the samples correspond to “highly proximal shelf”- and “heterolithic oxic shelf”-environments (fig. 4.8).

Unit C (119.05 m – 99 m)

This smaller unit of approximately 20 m thickness contained heterolithic deposits with interbeds of sand, mud, silt and coal debris (fig. 4.4). It is interpreted as delta sand flat deposits. Wave ripple cross lamination in the lower part indicates marine influence. A transition over to low-angle cross-stratified strata in the upper part most likely represent the shallower and subaerially exposed part of the sand flat. The medium grained sandstone indicates a relatively proximal position to fluvial sources. However, the sedimentologic analysis of this unit revealed no evidence of bioturbation and no presence of marine acritarchs were recorded from the quantitative palynology. Observations of the particulate organic matter indicate a strong terrestrial signature, in which the whole unit is dominantly composed of phytoclasts (fig. 5.4). Based on the information provided by the APP ternary plot, the composition of the particulate organic matter in these deposits are consistent with deposition between “highly proximal shelf”- and “heterolithic oxic shelf”-environments.

Unit D (99 m – 4 m)

This uppermost unit is distinguished from the underlying unit C primarily by a much higher mud-content (fig. 4.5). The palynofacies analysis reveals a cyclic trend within these deposits, ranging between AOM to phytoclast dominated assemblages (fig. 5.4). The presence of AOM typically indicates deposition under oxygen deficient conditions (Tyson, 1995, p. 249). However, an overall dominance of phytoclasts throughout this unit indicates a terrestrial environment. Additionally, the combined presence of bioturbation (high degree), bivalves, root horizons and coal beds indicate an environment frequently prone to marine processes

and periodic subaerial exposure (fig. 4.1). This unit represents a series of stacked parasequences separated by flooding surfaces. These sequences typically form coarsening and shallowing upward deposits grading from marine to shoreface, and into coastal plain deposits on top. Trace fossils and escape structures were observed and classified to *Diplocraterion*, which is typically present in intertidal and shallow subtidal environments (Zonneveld et al., 2001). The mud dominated beds has been interpreted to represent interdistributary bay deposits, periodically subjected to tidal influence, followed by swamp/marsh formation and deposition of root horizons and coal. The sedimentation pattern in interdistributary bays is mostly controlled by overbank spilling of fine-grained material from the distributary channel during flood stages (Bhattacharya, 2006). The high mud-content typically recorded in interdistributary bay-deposits may be punctuated by sandy crevasse-splays or channel deposits that may produce thin successions (Elliott, 1974). The succession may grade into rooted coaly mudstones or coals representing a variety of swamp, marsh and lacustrine environments (Bhattacharya, 2006), which fits the observations done in this uppermost unit of core 7534/4-U-1.

This environment typically reflects humid and damp conditions, which correlates well with the high occurrence of the fern spore *Leschikisporis aduncus* recorded at 25.63 m. The parent plant of this taxon prefers these warm conditions, and is typically found in swamps/marshes (Hochuli and Vigran, 2010; Paterson and Mangerud, 2015; Paterson et al., submitted). However, the dominance of the cavate spore genus Krauselisporites was also recorded within this unit. The complexity of this unit is also reflected in the APP ternary plot (fig. 4.8). The POM abundances recorded from this interval plot within a large range of environments, indicating frequent fluctuations between a marine to terrestrial, and oxic to anoxic signature.

Summary

Core 7534/4-U-1 has been interpreted to represent pro-delta to lower delta plain deposits. Each sample has been plotted on an AOM-Phytoclast-Palynomorph ternary plot, which visualize the fluctuations of proximity to terrestrial kerogen sources (fig. 4.8). According to

Tyson (1995) these assemblages correspond with “distal suboxic-anoxic”, “Heterolithic oxic” to “highly proximal” palaeoenvironments. The Spore-Pollen-Microplankton ternary plot confirms an environmental change from nearshore-offshore to fluvio-deltaic depositional environments (fig. 4.9). The overall dominance of terrestrial taxa, many of which are associated with swampy environments (e.g. *Leschikisporis aduncus* and *Aratrisporites* spp.), combined with minor occurrences of marine acritarchs indicates a coastal environment. The combined evidence from the core description, palynofacies and quantitative palynology thereby fit well together.

Hochuli and Vigran (2010) also documented an increasing abundance and diversity of fern spores in the Late Triassic. According to these authors, this trend represents a change from dryer conditions in the early Carnian (Floral Phase 10 and 11) to humid conditions from the ‘mid’ Carnian and onwards (Floral Phase 12 to 20)(fig. 5.1). This change is reflected in the palynoflora (Hochuli and Vigran, 2010), and could also be reflected in core 7534/4-U-1. Taxa typically associated with humid and warm conditions (e.g. *Leschikisporis aduncus* and *Dictyophyllidites mortonii*) were recorded in increased abundance in the uppermost part of the core (Assemblage SB-III), assigned a ‘mid’-late Carnian age, and could reflect this climatic change.

The erosional boundary at 152.80 m was proposed by Riis et al. (2008) to represent a hiatus and possibly correspond to the Ladinian-Carnian boundary. The present study supports this, although no confident conclusion could be reached based on palynology. The palynological assemblages recorded above and beneath this boundary is significantly different, but holds mainly long-ranging taxa diagnostic for both the Carnian and the Ladinian. The abrupt change from a marine environment into a terrestrially dominated channel system still suggests a hiatus of some timespan between these units (unit A and B/Assemblage SB-I and SB-II).

6. Conclusions

Palynostratigraphy

Core 7534/4-U-1 is assigned a late Ladinian to mid-late Carnian age based on correlation to previously established zonations by Hochuli et al. (1989), Mørk et al. (1990), Vigran et al. (1998), Hochuli and Vigran (2010), Vigran et al. (2014) and Paterson and Mangerud (2015). Concluding remarks:

- The presence of *Aulisporites astigmosus* (upper two assemblages) and *Echinitosporites iliacoides* suggests an overlap between the Carnian "*Aulisporites astigmosus* CAZ" and the Ladinian "*Echinitosporites iliacoides* CAZ" of Vigran et al. (2014) for core 7534/4-U-1.
- Absence of the taxa *Cordaitina gunyalensis, Bhardwajispora labichensis, Dyupetalum* cf. *vicentinensis* and *Jugasporites* spp. indicates a younger age than the early Ladinian "Assemblage I" of Hochuli et al. (1989) and "Svalis-8" of Vigran et al. (1998) for the lowermost part of core 7534/4-U-1.
- An early Carnian age can be assigned to the middle assemblage SB-II based on good correlation to "Assemblage F" of Hochuli et al. (1989), "Floral Phase 11" of Hochuli and Vigran (2010) and the Kong Karls Land assemblage of Paterson et al. (submitted).
- A mid-late Carnian age can be assigned to the uppermost assemblage SB-III based on good correlation to "Assemblage D and E" of Hochuli et al. (1989), "Floral Phase 12" of Hochuli and Vigran (2010), "*Aulisporites astigmosus* Zone" of Vigran et al. (2014) and the "*Leschikisporis aduncus* assemblage" of Paterson and Mangerud (2015).
- The succession predates the latest Carnian "*Protodiploxypinus* spp. assemblage" of Paterson and Mangerud (2015), "Assemblage C" of Hochuli et al. (1989) and the "*Rhaetogonyaulax* spp. CAZ" of Vigran et al. (2014).
- Absence of dinoflagellate cysts indicates a pre-Norian age for core 7534/4-U-1.

Palaeoenvironment

Core 7534/4-U-1 has been interpreted to represent pro-delta to lower delta plain deposits.

- Varying presence of marine acritarchs suggest prevalent to episodic marine influence, which is reflected by the finely laminated pro-delta shales, and the heterolithic lower delta plain deposits, respectively. Palynofacies estimates indicate periodically reducing conditions based on the dominance of AOM in some intervals, often associated with marine environments.
- An overall dominance of terrestrial taxa indicates a close proximity to terrestrial plant communities, often represented in coastal environments.
- The high abundance of the fern spores *Leschikisporis aduncus, Deltoidospora* spp. and *Dictyophyllidites mortonii* indicates humid conditions, and are often associated with swamp/marsh environments (as described by Hochuli and Vigran. 2010). Such conditions are typically found on delta plains.
- The changes in facies associations are well represented by the APP and SPM ternary plots, and confirms an upward change from nearshore/offshore- to fluvio-deltaic environments in core 7534/4-U-1.
- This combined dataset of core 7534/4-U-1 reflects the Carnian evolution of the vast delta system prograding over the Barents Sea Shelf, as documented by Riis et al. (2008).

References

Ask, M. (2013). Palynological dating of the upper part of the De Geerdalen Formation on central parts of Spitsbergen and Hopen. (Msc. thesis), University of Bergen, Norway, pp. 1-79.

Bhattacharya, J. P. (2006). Deltas. *SPECIAL PUBLICATION-SEPM, 84*, 237.

Bjærke, T. (1977). Mesozoic palynology of Svalbard II. Palynomorphs from the Mesozoic sequence of Kong Karls Land. *Norsk Polarinstitutt Årbok 1976*, 83-120.

Bjærke, T., & Dypvik, H. (1977). Sedimentological and palynological studies of Upper Triassic-Lower Jurassic sediments in Sassenfjorden, Spitsbergen. *Norsk Polarinstitutt Årbok 1976*, 131-150.

Bjærke, T., & Manum, S. B. (1977). Mesozoic palynology of Svalbard. I, The Rhaetian of Hopen, with a preliminary report on the Rhaetian and Jurassic of Kong Karls Land.

Bonis, N., Kürschner, W., & Krystyn, L. (2009). A detailed palynological study of the Triassic–Jurassic transition in key sections of the Eiberg Basin (Northern Calcareous Alps, Austria). *Review of Palaeobotany and Palynology, 156*(3), 376-400.

Buchan, S., Challinor, A., Harland, W., & Parker, J. (1965). The Triassic stratigraphy of Svalbard.

Cirilli, S. (2010). Upper Triassic–lowermost Jurassic palynology and palynostratigraphy: a review. *Geological Society, London, Special Publications, 334*(1), 285-314.

Coleman, J. M., & Wright, L. (1975). Modern river deltas: variability of processes and sand bodies.

Combaz, A. (1964). Les palynofacies. *Revue de Micropaléontologie, 7*(3), 205-218.

Duringer, P., & Doubinger, J. (1985). La palynologie: un outil de caractérisation des faciès marins et continentaux à la limite Muschelkalk supérieur Lettenkohle. *Sci. Géol. Bull, 38*(1), 19-34.

Elliott, T. (1974). Interdistributary bay sequences and their genesis. *Sedimentology, 21*(4), 611-622.

Elliott, T. (1986). Deltas. *Sedimentary environments and facies, 2*, 113-154.

Federova, V. (1977). The significance of the combined use of microphytoplankton, spores, and pollen for differentiation of multi-facies sediments. *In Questions of phttostratigraphy. Trudy Neftyanoi nauchno-issledovatelskii geologo-razvedochnyi Institute (VNIGRI) Leningrad, 398*, 70-88.

Felix, C. J. (1975). Palynological evidence for Triassic sediments on Ellef Ringnes Island, Arctic Canada. *Review of Palaeobotany and Palynology, 20*(1), 109-117.

Fisher, M. (1972). The Triassic palynofloral succession in England. *Geoscience and Man, 4*(1), 101-109.

Fisher, M. (1979). The Triassic palynofloral succession in the Canadian Arctic Archipelago. *American Association of Stratigraphic Palynologists Contribution Series 5B*, 83-100.

Fisher, M., & Bujak, J. (1975). Upper Triassic palynofloras from arctic Canada. *Geoscience and man, 11*(1), 87-94.

Glørstad-Clark, E., Birkeland, E., Nystuen, J., Faleide, J., & Midtkandal, I. (2011). Triassic platform-margin deltas in the western Barents Sea. *Marine and Petroleum Geology, 28*(7), 1294-1314.

Glørstad-Clark, E., Faleide, J. I., Lundschien, B. A., & Nystuen, J. P. (2010). Triassic seismic sequence stratigraphy and paleogeography of the western Barents Sea area. *Marine and Petroleum Geology, 27*(7), 1448-1475.

Hochuli, P., Colin, J., & Vigran, J. O. (1989). Triassic biostratigraphy of the Barents Sea area *Correlation in hydrocarbon exploration* (pp. 131-153): Springer.

Hochuli, P. A., & Frank, S. M. (2000). Palynology (dinoflagellate cysts, spore-pollen) and stratigraphy of the Lower Carnian Raibl Group in the Eastern Swiss Alps. *Eclogae Geologicae Helvetiae, 93*(3), 429-443.

Hochuli, P. A., & Vigran, J. O. (2010). Climate variations in the Boreal Triassic—inferred from palynological records from the Barents Sea. *Palaeogeography, Palaeoclimatology, Palaeoecology, 290*(1), 20-42.

Holen, L. H. (2014). Late Triassic (Carnian) Palynology of the Northern Barents Sea (Sentralbanken High). (Msc. thesis), University of Bergen, Norway, pp. 1-96.

Høy, T., & Lundschien, B. (2011). Triassic deltaic sequences in the northern Barents Sea. *Geological Society, London, Memoirs, 35*(1), 249-260.

Klaus, W. (1960). *Sporen der karnischen Stufe der ostalpinen Trias*: na.

Klausen, T. G., Ryseth, A. E., Helland-Hansen, W., Gawthorpe, R., & Laursen, I. (2015). Regional development and sequence stratigraphy of the Middle to Late Triassic Snadd Formation, Norwegian Barents Sea. *Marine and Petroleum Geology, 62*, 102-122.

Korchinskaya, M. (1980). Rannenorijskaja fauna archipelaga Sval'bard.(Early Norian fauna of the archipelago of Svalbard.). *Geologija osadoč nogo č echla archipelaga Sval'bard.(Geology of the sedimentary platform cover of the archipelago of Svalbard.): Leningrad, NIIGA*, 30-43.

Kürschner, W. M., & Herngreen, G. W. (2010). Triassic palynology of central and northwestern Europe: a review of palynofloral diversity patterns and biostratigraphic subdivisions. *Geological Society, London, Special Publications, 334*(1), 263-283.

Lundschien, B. A., Høy, T., & Mørk, A. (2014). Triassic hydrocarbon potential in the Northern Barents Sea; integrating Svalbard and stratigraphic core data. *Norwegian Petroleum Directorate Bulletin, 11*, 3-20.

Mertens, K. N., Verhoeven, K., Verleye, T., Louwye, S., Amorim, A., Ribeiro, S., Deaf, A. S., Harding, I. C., De Schepper, S., & González, C. (2009). Determining the absolute abundance of dinoflagellate cysts in recent marine sediments: the Lycopodium marker-grain method put to the test. *Review of Palaeobotany and Palynology, 157*(3), 238-252.

Mørk, A., Dallmann, W., Dypvik, H., Johannessen, E., Larssen, G., Nagy, J., Nøttvedt, A., Olaussen, S., Pchelina, T., & Worsley, D. (1999). Mesozoic lithostratigraphy. *Lithostratigraphic lexicon of Svalbard. Upper Palaeozoic to Quaternary bedrock. Review and recommendations for nomenclature use*, 127-214.

Mørk, A., Vigran, J. O., & Hochuli, P. A. (1990). Geology and palynology of the Triassic succession of Bjørnøya. *Polar Research, 8*(2), 141-163.

Nagy, J., Hess, S., Dypvik, H., & Bjærke, T. (2011). Marine shelf to paralic biofacies of Upper Triassic to Lower Jurassic deposits in Spitsbergen. *Palaeogeography, Palaeoclimatology, Palaeoecology, 300*(1), 138-151.

Ogg, J. G., Ogg, G., & Gradstein, F. M. (2008). *The concise geologic time scale* (Vol. 1).

Os Vigran, J., Mangerud, G., Mørk, A., Bugge, T., & Weitschat, W. (1998). Biostratigraphy and sequence stratigraphy of the Lower and Middle Triassic deposits from the Svalis Dome, central Barents Sea, Norway. *Palynology, 22*(1), 89-141.

Paterson, N. W., & Mangerud, G. (2015). Late Triassic (Carnian–Rhaetian) palynology of Hopen, Svalbard. *Review of Palaeobotany and Palynology*.

Paterson, N. W., Mangerud, G., Lundschien, B. A., Mørk, A. (submitted). Late Triassic (early Carnian) palynology of shallow stratigraphic core 7830/5-U-1, offshore Kong Karls Land, Norwegian Arctic.

Pautsch, M. E. (1973). Upper Triassic spores and pollen from the Polish Carpathian Foreland. *Micropaleontology*, 129-149.

Riis, F., Lundschien, B. A., Høy, T., Mørk, A., & Mørk, M. B. E. (2008). Evolution of the Triassic shelf in the northern Barents Sea region. *Polar Research, 27*(3), 318-338.

Smith, D. G. (1974). Late Triassic pollen and spores from the Kapp Toscana Formation, Hopen, Svalbard—a preliminary account. *Review of Palaeobotany and Palynology, 17*(1), 175-178.

Smith, D. G. (1982). Stratigraphic significance of a palynoflora from ammonoidbearing Early Norian strata in Svalbard. *Newsletters on Stratigraphy*, 154-161.

Smith, D. G., Harland, W., & Hughes, N. (1975). Geology of Hopen, Svalbard. *Geological Magazine, 112*(01), 1-23.

Tozer, E. T. (1961). *Triassic stratigraphy and faunas, Queen Elizabeth Islands, Arctic Archipelago*: Department of Mines and Technical Surveys.

Tozer, E. T., & Tozer, E. (1967). *A standard for Triassic time*: Department of Energy, Mines and Resources.

Traverse, A. (1988). Paleopalynology. 600 pp: Boston.

Traverse, A. (2007), Paleopalynology, The Netherlands, Springer, v. 2nd edition.

Tyson, R. (1989). Late Jurassic palynofacies trends, Piper and Kimmeridge Clay formations, UK onshore and northern North Sea. *Northwest European micropalaeontology and palynology*, 135-172.

Tyson, R. (1995). Sedimentary organic matter: organic facies and palynofaciesChapman and Hall. *London, New York*.

Tyson, R. V. (1985). *Palynofacies and sedimentology of some Late Jurassic sediments from the British Isles and northern North Sea.* Open University.

Tyson, R. V. (1993). Palynofacies analysis *Applied micropalaeontology* (pp. 153-191): Springer.

Van der Eem, J. (1983). Aspects of Middle and Late Triassic palynology. 6. Palynological investigations in the Ladinian and Lower Karnian of the western Dolomites, Italy. *Review of Palaeobotany and Palynology, 39*(3), 189-300.

Vigran, J., Mangerud, G., Mørk, A., Worsley, D., & Hochuli, P. (2014). Palynology and geology of the Triassic succession of Svalbard and the Barents Sea. *Geological Survey of Norway Special Publication, 14*, 1-270.

Worsley, D. (2008). The post-Caledonian development of Svalbard and the western Barents Sea. *Polar Research, 27*(3), 298-317.

Worsley, D., Johansen, R., & Kristensen, S. (1988). The Mesozoic and Cenozoic succession of Tromsøflaket. *A lithostratigraphic scheme for the Mesozoic and Cenozoic succession offshore mid-and northern Norway. Norwegian Petroleum Directorate Bulletin, 4*, 42-65.

Zonneveld, J.-P., Gingras, M., & Pemberton, S. (2001). Trace fossil assemblages in a Middle Triassic mixed siliciclastic-carbonate marginal marine depositional system, British Columbia. *Palaeogeography, Palaeoclimatology, Palaeoecology, 166*(3), 249-276.

Appendices

Appendix I: List of recorded taxa

Appendix II: Combined range chart of core 7534/4-U-1

Appendix III: Plates

Appendix I - List of recorded taxa

Spores

Anapiculatisporites spp.	
Anapiculatisporites spininger	(Leschik, 1955) Reinhardt, 1962
Annulispora folliculosa	(Rogalska) de Jersey, 1959
Apiculatisporites spp.	
Apiculatisporites parvispinosus	(Leschik) Playford and Dettman, 1965
Aratrisporites spp.	
Aratrisporites laevigatus	Bjærke and Manum, 1977
Aratrisporites macrocavatus	Bjærke and Manum, 1977
Aratrisporites scabratus	Klaus, 1960
Baculatisporites spp.	
Calamospora tener	(Leschik) Mädler, 1964
Camarozonosporites spp.	
Camarozonosporites rudis	(Leschik) Klaus, 1960
Clathroidites spp.	
C*onbaculatisporites* spp.	
Conbaculatisporites hopensis	Bjærke and Manum, 1977
Concavisporites spp.	
Converrucosisporites spp.	
Cyclotriletes spp.	
Deltoidospora spp.	
Densosporites spp.	
Dictyophyllidites mortonii	(de Jersey) Playford and Dettman, 1965
Duplexisporites problematicus	(Couper) Playford and Dettman, 1965
Krauselisporites spp.	
Krauselisporites apiculatus	Jansonius, 1962
Krauselisporites cooksonae	(Klaus) Dettman, 1963
Krauselisporites dendatus	Leschik, 1956
Kyrtomisporis spp.	
Kyrtomisporis cf. *laevigatus*	

Leschikisporis aduncus (Leschik) Potonié, 1958

Limatulasporites limatulus (Playford) Helby and Foster, 1979

Polycingulatisporites spp.

Porcellispora longdonensis (Clarke) Scheuring, 1970 emend. Morbey, 1975

Punctatisporites spp.

Retriletes spp.

Retusotriletes spp.

Stereisporites spp.

Striatella spp.

Striatella parva (Li and Shang) Filatoff and Price, 1988

Striatella seebergensis Mädler, 1964

Thomsonisporites spp.

Thomsonisporites toralis Leschik, 1955

Verrucosisporites spp.

Zebrasporites spp.

Zebrasporites fimbriatus Klaus, 1960

Zebrasporites interscriptus (Thiergart) Klaus, 1960

Pollen

Alisporites spp.

Angustisulcites klausii (Freudenthal) Visscher, 1966

Aulisporites astigmosus (Leschik) Klaus, 1960

Araucariacites australis Cookson, 1947

Bisaccate spp. (indeterminate)

Chasmatosporites spp.

Chasmatosporites apertus (Rogalska) Nilsson, 1958

Chasmatosporites hians Nilsson, 1958

Classopollis torosus (Reissinger) Klaus, 1960 emend. Cornet & Traverse, 1975

Cordaitina minor

Cycadopites spp. Wodehouse, 1933

Echinitosporites iliacoides Schulz, 1961

Granasporites spp.

Illinites chitinoides	Klaus, 1964
Institisporites crispus	Pautsch, 1971
Lunatisporites spp.	
Ovalipollis spp.	
Ovalipollis ovalis	(Krutsch) Scheuring, 1970
Ovalipollis pseudoalatus	(Thiegart) Schuurman, 1976
Podosporites spp.	
Podosporites amicus	Scheuring, 1970
Protodiploxypinus spp.	
Protodiploxypinus ornatus	(Pautsch) Bjærke and Manum, 1977
Protodiploxypinus microsaccus	
Protodiploxypinus minor	Bjærke and Manum, 1977
Quadraeculina anellaeformis	Maljavkina, 1949
Riciisporites umbonatus	Felix and Burbridge, 1977
Schizaeoisporites worsleyi	Bjærke and Manum, 1977
Staurosaccites quadrifidus	Dolby and Balme, 1976
Steevesipollenites spp.	
Striatoabieites spp.	
Striatoabieites balmei	(Klaus) Scheuring, 1978
Striatoabieites multistriatus	(Balme and Hennelly) Hart, 1964
Triadispora spp.	
Triadispora obscura	Scheuring, 1970
Triadispora verrucata	(Schulz) Scheuring, 1970
Vesicasporis fuscus	(Pautsch) Morbey, 1975
Vitreisporites pallidus	(Reissinger) Nilsson, 1958

Acritarchs

Leiosphaeridia spp.

Michrystridium spp.

Veryhachium spp.

Dictyotidium spp.

Prasinophytes

Cymatiosphaera spp.

Chlorococcales

Botrycoccus	Ktzing, 1849
Crassospaera spp.	
Plaesiodictyon mosellaneum	Willie, 1970

Appendix II – Range Chart

Relative abundances of recorded palynomorphs from core 7534/4-U-1, including palynofacies estimates and cropped core log (A3 size-format required when printed).

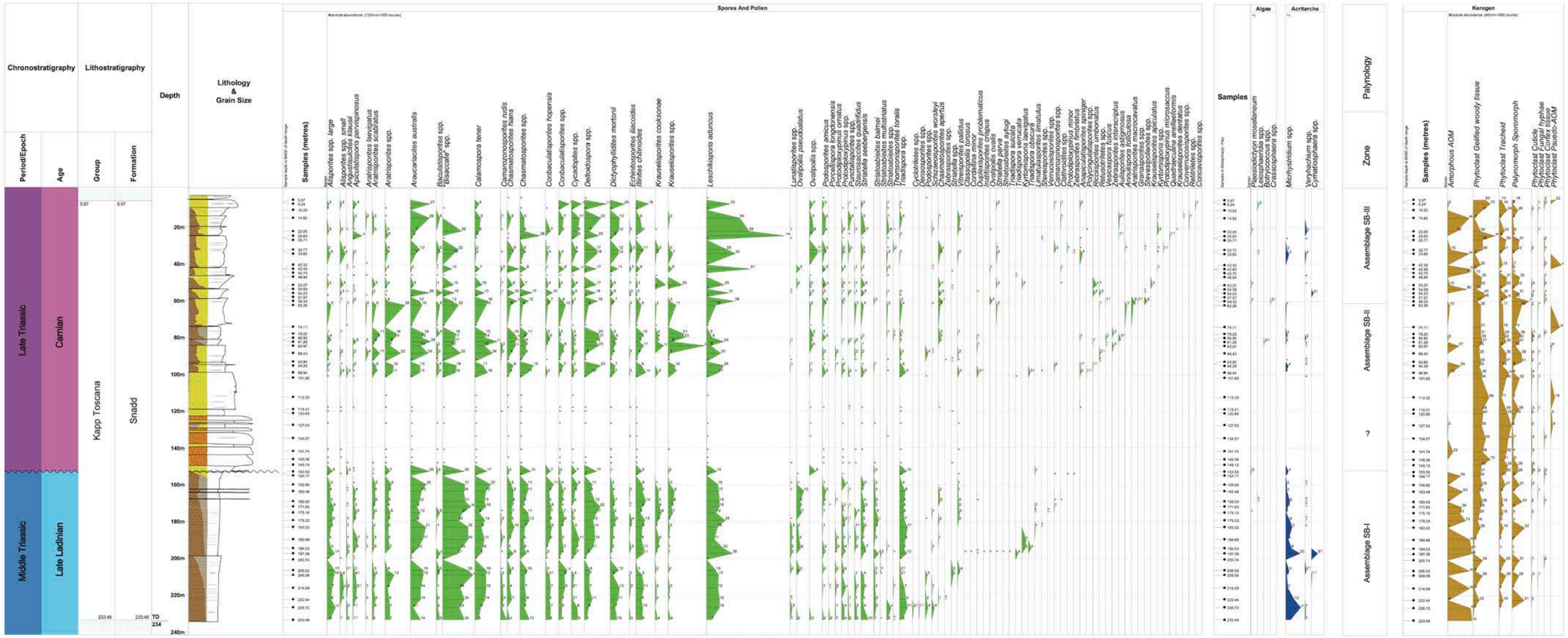

Appendix III - Plates

Plates of selected species recorded from core 7534/4-U-1. The species/genus are followed by the sample depth. Two samples were often provided for the same sample depth resembling first and second oxidations. Slide information is given by 'O' or 'O^{2}' in this case. England Finder coordinates are provided for all the presented taxa. The slides were inspected under the microscope with the label to the left. A 20-µm scale is included for each specimen.

Plate I

Fig. 1: *Anapiculatisporites spiniger* 42.49 m (O), V19-4

Fig. 2: *Apiculatisporis parvispinosus* 32.77 m (O), Q28-3

Fig. 3: *Annulispora folliculosa* 32.77 m, J17

Fig. 4: *Aratrisporites laevigatus* 78.22 m, O33-2

Fig. 5: *Aratrisporites scabratus* 14.82 m (O^2), Q33-4

Fig. 6: *Aratrisporites* spp. 194.53 m, O18-2

Fig. 7: *Aratrisporites* spp. 194.53 m, N23-4

Fig. 8: *Zebrasporites fimbriatus* 33.60 m (O), V29

Fig. 9: *Zebrasporites interscriptus* 78.22 m, O36

Fig. 10: *Baculatisporites* spp. 194.53 m, N28

Plate I

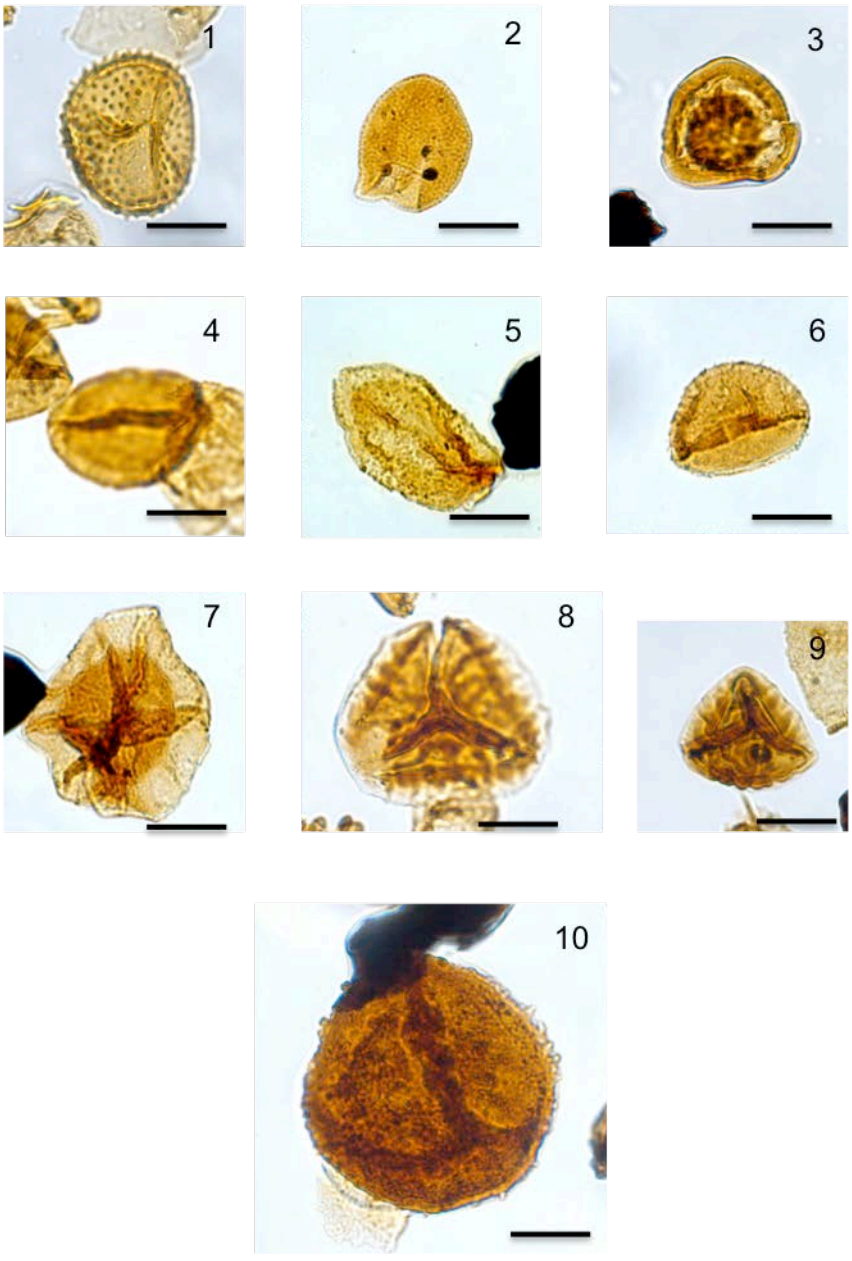

Plate II

Fig. 1: *Calamospora tener* 59.33 m, Y40-1

Fig. 2: *Camarozonosporites rudis* 78.22 m, L23-4

Fig. 3: *Camarozonosporites rudis* 32.77 m (O), D26-2

Fig. 4: *Camarozonosporites* spp. 233.48 m (O^2), P16-2

Fig. 5: *Conbaculatisporites* spp. 194.53 m, N31-3

Fig. 6: *Conbaculatisporites hopensis* 194.53 m, N27-4

Fig. 7: *Deltoidospora* spp. 194.53 m, N38-3

Fig. 8: *Deltoidospora* spp. 32.77 m (O), Q28-4

Fig. 9: *Dictyophyllidites mortonii* 59.33 m, Y26

Fig. 10: *Dictyophyllidites mortonii* 42.49 m (O), V19-4

Fig. 11: *Krauselisporites* spp. 83.97 m, N34-2

Fig. 12: *Krauselisporites cooksonae* 83.97 m, L20-3

Plate II

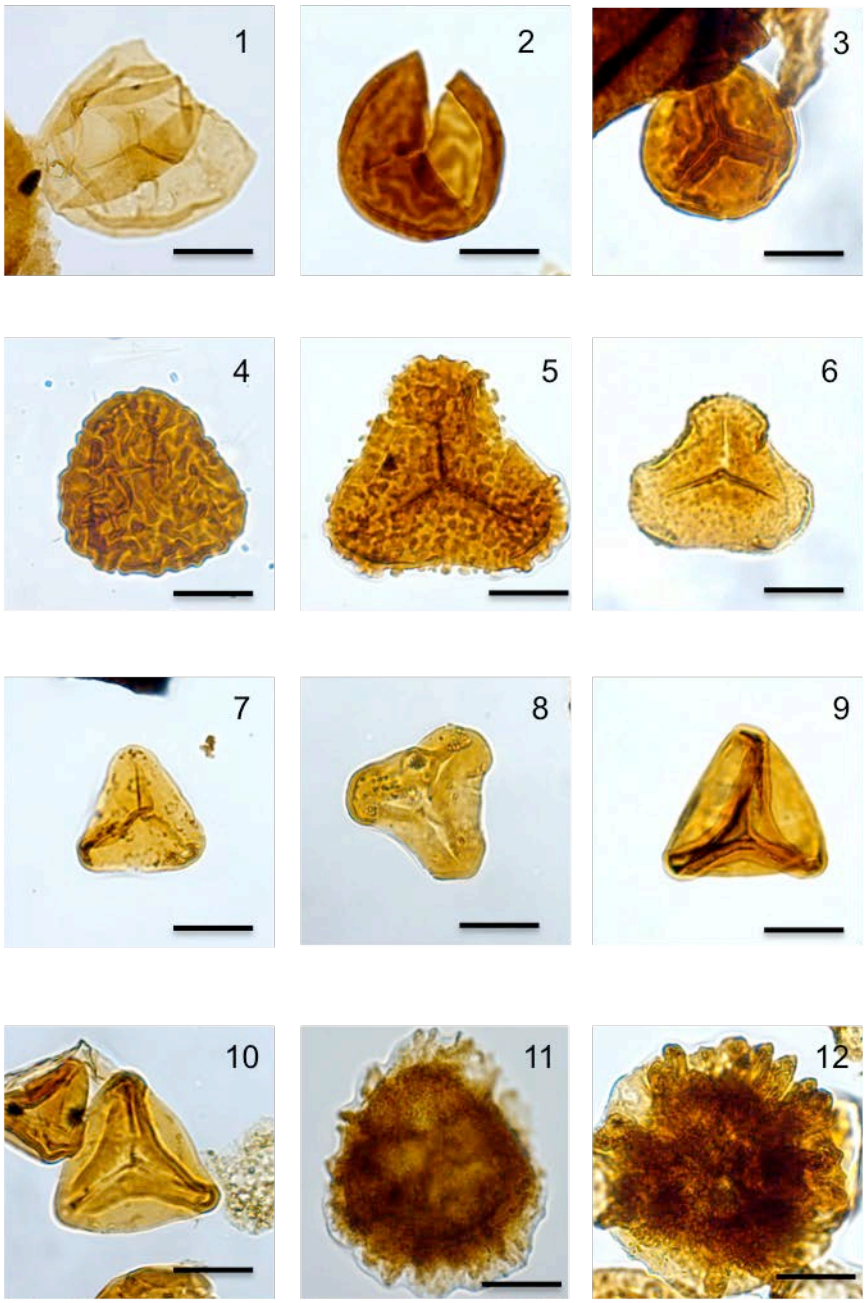

Plate III

Fig. 1: *Kyrtomisporis* spp. 53.27 m (O^2), K34-3

Fig. 2: *Striatella* spp. 33.77 m (O), Q28-4

Fig. 3: *Striatella seebergensis* 169.0 m, R22-3

Fig. 4: *Striatella seebergensis* 183.02 m, V12-3

Fig. 5: *Punctatisporites* spp. 54.23 m, M38-1

Fig. 6: *Duplexisporites problematicus* 169.0 m, X30-2

Fig. 7: *Leschikisporis aduncus* 59.33 m, Y33-2

Fig. 8: *Limatulasporites limatulus* 153.55 m, P42

Fig. 9: *Stereisporites* spp. (?) 183.02 m, T11-4

Fig. 10: *Pocellispora longdonensis* 233.48 m (O^2), U18-4

Fig. 11: *Retriletes* spp. 59.33 m, X35

Plate III

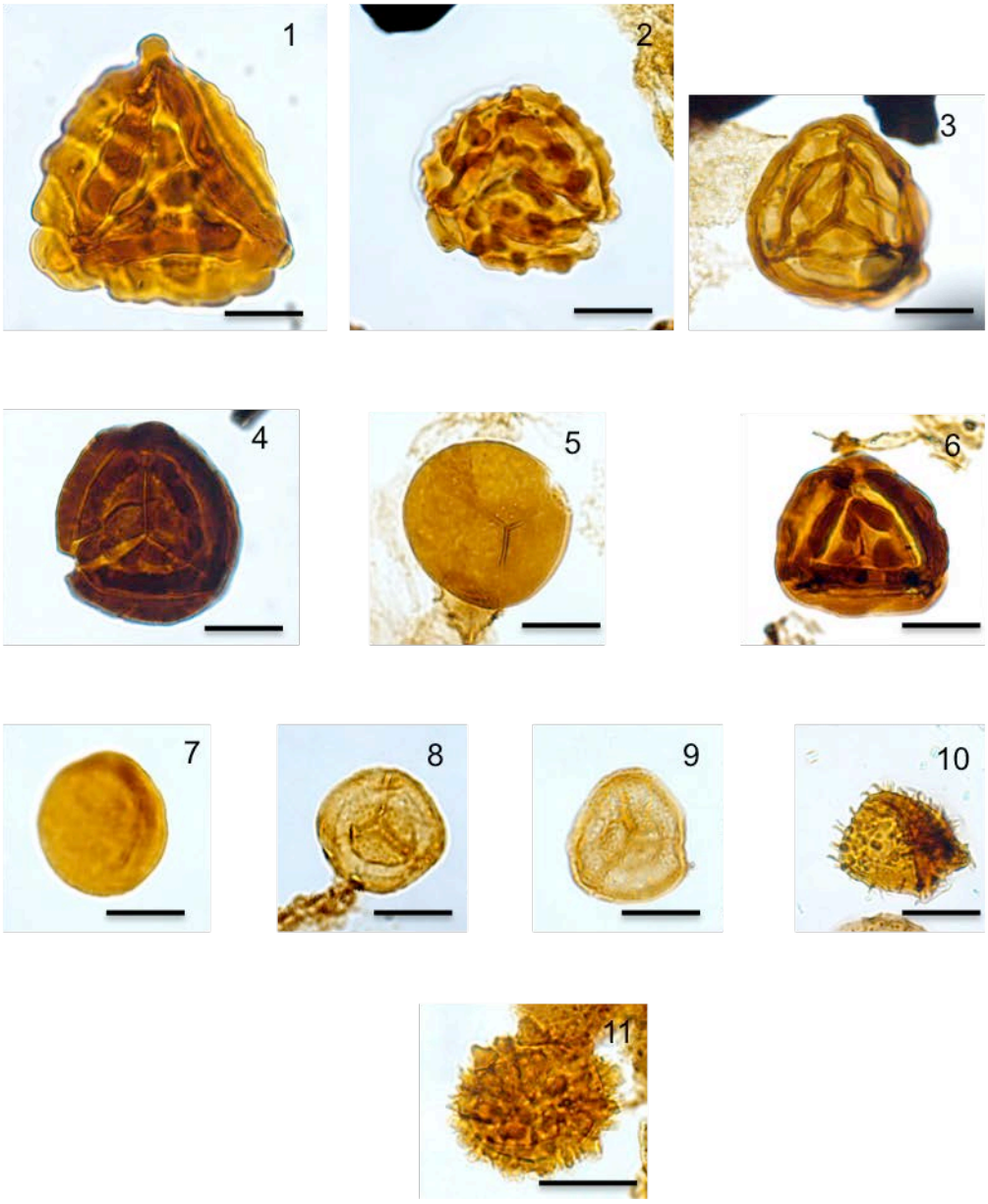

Plate IV

Fig. 1: *Ovalipollis ovalis* 6.24 m (O), P25-1

Fig. 2: *Illinites chitinoides* 98.94 m, U35-4

Fig. 3: *Araucariacites australis* 54.23 m, L22-4

Fig. 4: *Chasmatosporites hians* 194.53 m, N25-3

Fig. 5: *Chasmatosporites apetus* 197.38 m, H21-3

Fig. 6: *Cycadopites* spp. 80.90 m, M33

Fig. 7: *Echinitosporites iliacoides* 22.05 m, O23

Fig. 8: *Aulisporites astigmosus* 14.82 m (O^2), U29

Fig. 9: *Lunatisporites* spp. 216.09 m, K17

Fig. 10: *Alisporites* spp. 197.38 m, K20-4

Fig. 11: *Alisporites* spp. 163.48 m, H33-4

Plate IV

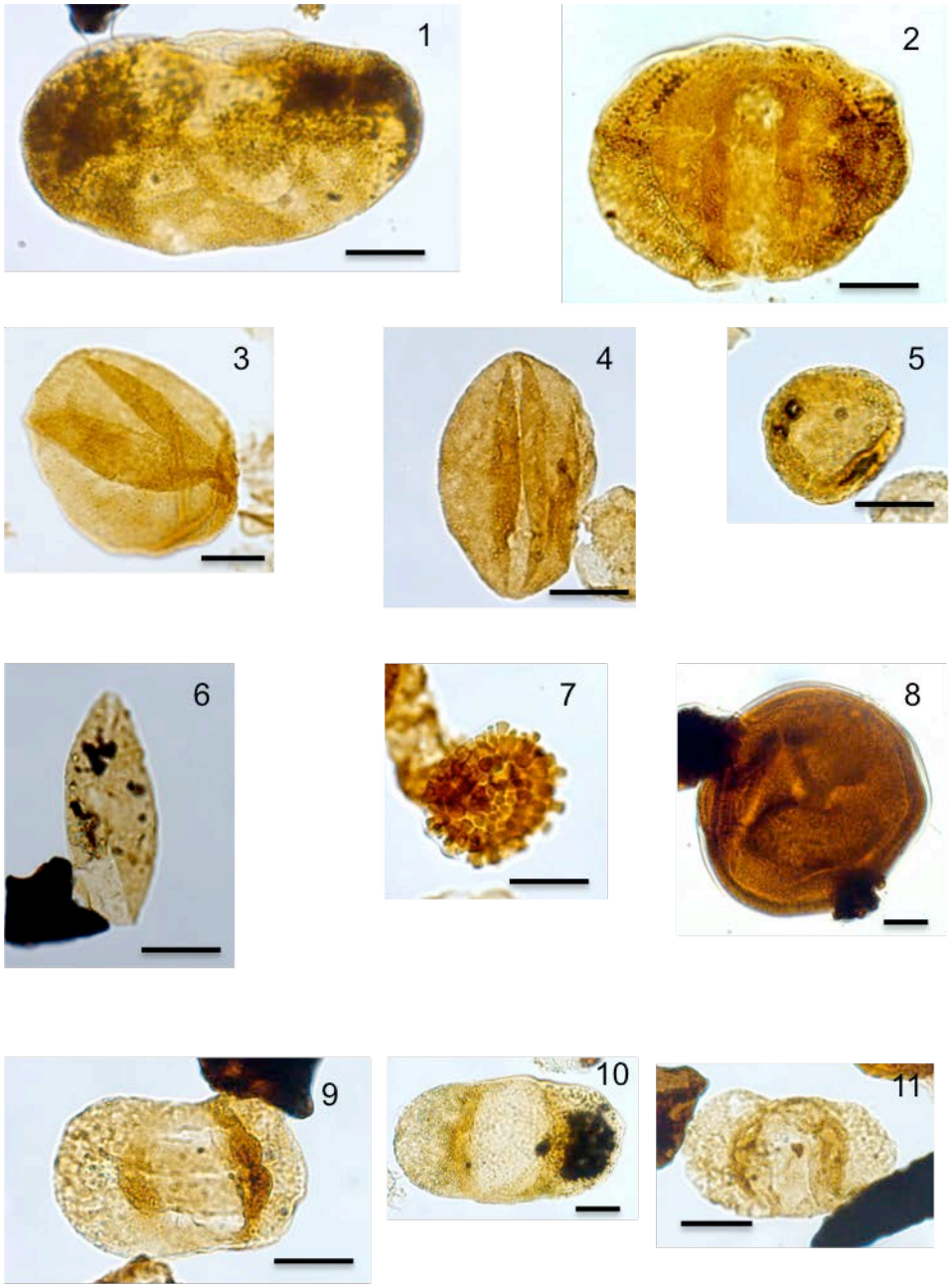

Plate V

Fig. 1: *Podosporites amicus* 163.48 m, H25-1

Fig. 2: *Protodiploxypinus* spp. 169.0 m, U34-3

Fig. 3: *Institisporites crispus* 197.38 m, P32-1

Fig. 4: *Angustisulcites klausii* 194.63 m, N26-2

Fig. 5: *Staurosaccites quadrifidus* 163.48 m, Q31

Fig. 6: *Striatoabieites balmei* 197.38 m, K35-2

Fig. 7: *Striatoabieites multistriatus* 194.53 m, Q31-4

Fig. 8: *Triadispora* spp. 183.02 m, P34-1

Fig. 9: *Triadispora* spp. 78.22 m, O37-1

Fig. 10: *Vitreisporites pallidus* 175.10 m, N33

Fig. 11: *Vesicaspora fuscus* 80.90 m, M36

Plate V

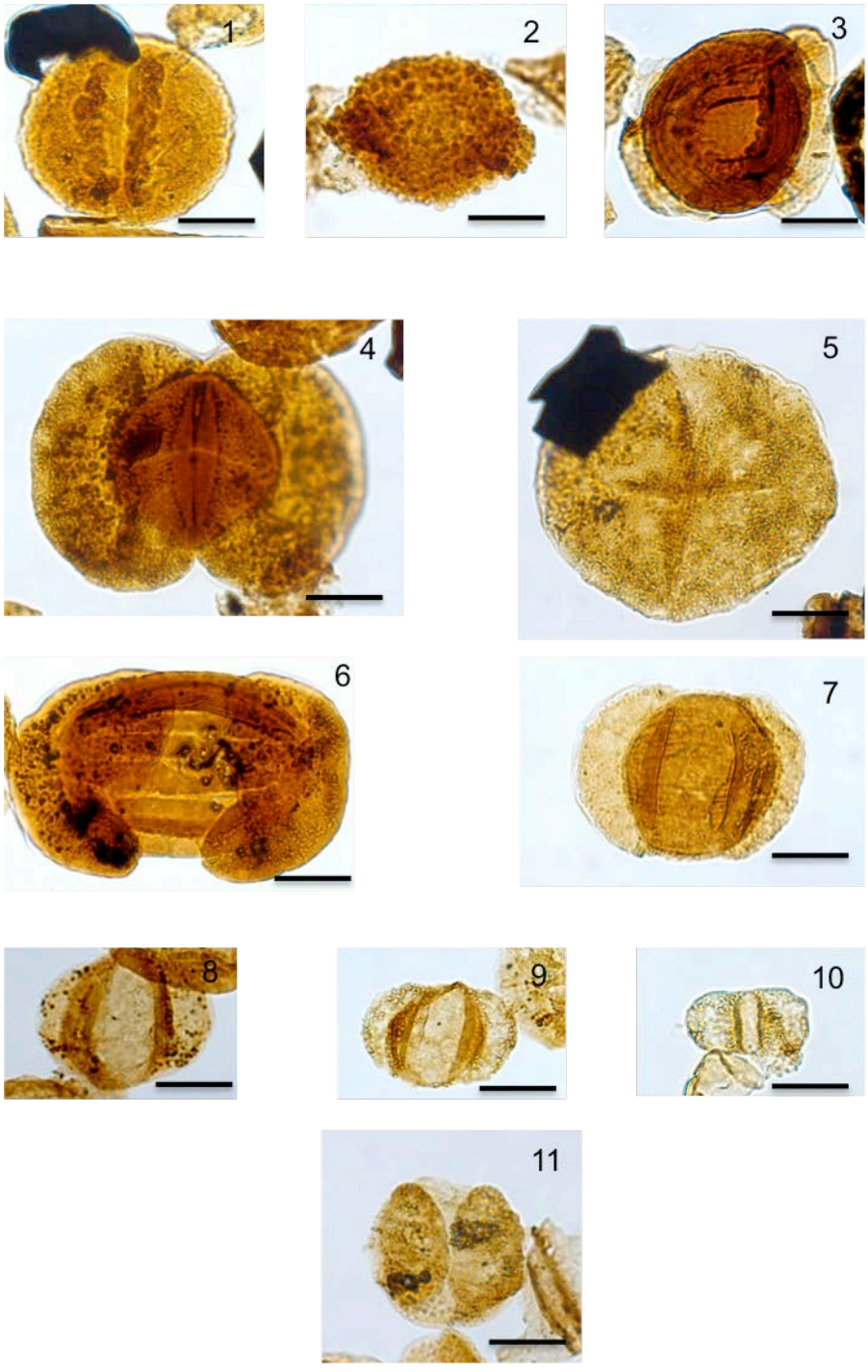

Plate VI

Fig. 1: *Michrystridium* spp. 169.0 m, X20-3

Fig. 2: *Cymatiosphaera* spp. 197.38 m, O30-2

Fig. 3: *Cymatiosphaera* spp. 197.38 m, H21-3

Fig. 4: *Veryhachium* spp. 226.72 m (O), S25-4

Fig. 5: *Veryhachium* spp. 233.48 m (O^2), P16-2

Plate VI